JGR Earth Surface

RESEARCH ARTICLE
10.1029/2019JF005359

Morainal Bank Evolution and Impact on Terminus Dynamics During a Tidewater Glacier Stillstand

E. F. Eidam[1], D. A. Sutherland[2], D. Duncan[3], C. Kienholz[4], J. M. Amundson[4], and R. J. Motyka[4,5]

[1]Department of Marine Sciences, University of North Carolina at Chapel Hill, Chapel Hill, NC, USA, [2]Department of Earth Sciences, University of Oregon, Eugene, OR, USA, [3]Institute for Geophysics, University of Texas at Austin, Austin, TX, USA, [4]Department of Natural Sciences, University of Alaska Southeast, Juneau, AK, USA, [5]Geophysical Institute, University of Alaska Fairbanks, Fairbanks, AK, USA

Abstract Sedimentary processes are known to help facilitate tidewater glacier advance, but their role in modulating retreat is uncertain and poorly quantified. In this study we use repeated seafloor bathymetric surveys and satellite-derived terminus positions from LeConte Glacier, Alaska, to evaluate the evolution of a morainal bank and related changes in terminus dynamics over a 17-year period. The glacier experienced a rapid retreat between 1994 and 1999, before stabilizing at a constriction in the fjord. Since then, the glacier terminus has remained stabilized while constructing a morainal bank up to 140 m high in water depths of 240–260 m, with rates of sediment delivery of 3.3×10^5 to 3.8×10^5 m^3 a^{-1}. Based on repeated interannual surveys between 2016 and 2018, the moraine is a dynamic feature characterized by push ridges, evidence of active gravity flows, and bulldozing by the glacier at rates of up to meters per day. Beginning in 2016, the summertime terminus has become increasingly retracted, revealing a newly emerging basin potentially signaling the onset of renewed retreat. Between 2000 and 2016, the growing moraine reduced the exposed submarine area of the terminus by up to 22%, altered the geometry of the terminus during seasonal advances, and altered the terminus stress balance. These feedbacks for calving, melting, and ice flow likely represent mechanisms whereby moraine growth may delay glacier retreat, in a system where readvance is unlikely.

Key Points:
- A new morainal bank up to 140 m high grew in 17 years at LeConte Glacier (southeast Alaska), during a glacier stillstand at a constriction
- Repeated multibeam surveys have highlighted dynamic processes of moraine sediment delivery, failure, and reworking by ice
- In cases where moraine development does not facilitate glacier readvance, it may still influence the retreat history

Supporting Information:
- Supporting Information S1

Correspondence to:
E. F. Eidam,
efe@unc.edu

Citation:
Eidam, E. F., Sutherland, D. A., Duncan, D., Kienholz, C., Amundson, J. M., & Motyka, R. J. (2020). Morainal bank evolution and impact on terminus dynamics during a tidewater glacier stillstand. *Journal of Geophysical Research: Earth Surface*, *125*, e2019JF005359. https://doi.org/10.1029/2019JF005359

Received 9 SEP 2019
Accepted 11 SEP 2020
Accepted article online 25 SEP 2020

1. Introduction

Tidewater glaciers are well known to undergo cycles of slow advance and rapid retreat, related to the interplay of climate, glacier, sediment, and ocean dynamics (e.g., Brinkerhoff et al., 2017; Meier & Post, 1987; Post, 1975; Stearns et al., 2015). While climatic changes have generally been linked to glacier retreat worldwide, the "tidewater glacier cycle" can obfuscate these signals because a few of these glaciers are presently advancing, out of phase with neighboring systems and regional temperature trends (Catania et al., 2018; McNabb & Hock, 2014; Motyka et al., 2017; Post et al., 2011). Thus, being able to better predict and model cycles of glacier advance and retreat is key to understanding longer–time scale climate forcings of glaciated systems.

In the tidewater glacier cycle, glaciers advance when the mass flux of ice to the terminus exceeds frontal ablation (iceberg calving plus submarine melting). This advance is often facilitated by the growth of a sedimentary shoal or "morainal bank complex" (henceforth referred to as MB), that is, an accumulation of till and glacifluvial sediments deposited at the grounding line and remobilized down-fjord by the advancing glacier. MBs play several key roles in supporting glacier advance: they shelter glacier termini from warm ocean water, reducing melting (e.g., Truffer & Motyka, 2016); they provide a shallow base for glacier termini, thereby reducing calving rates (e.g., Alley, 1991); and they provide a backstop, allowing glaciers to thicken (Amundson, 2016; Fischer & Powell, 1998). Actively advancing glaciers are known to push their MB ahead of them, maintaining this protective buffer/anchor (e.g., Hubbard Glacier, Goff et al., 2012; Kuriger et al., 2006; Motyka et al., 2006; Taku Glacier, Nolan et al., 1995). Over time, as the accumulation-area ratio (the ratio of the accumulation area to the total glacier area; AAR) of the glacier decreases, the glacier mass balance will become insufficient to maintain advance. Subsequent thinning and retreat from the MB into an overdeepened basin will expose the ice front to greater water depths and thus increase the potential for iceberg calving and submarine melting (e.g., Alley, 1991; Truffer & Motyka, 2016; van der Veen, 1996).

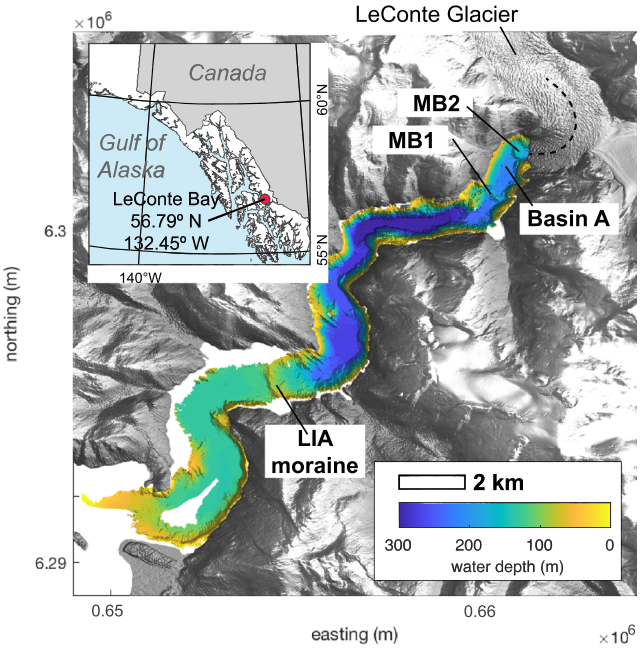

Figure 1. Vicinity map. LeConte Bay is a fjord carved by LeConte Glacier in southeast Alaska. Data are from 2016 survey (this study). The dashed line approximates the central flowline of the glacier upstream of the present terminus.

Rapid retreat often follows—for example, several kilometers in a few years (McNabb & Hock, 2014)—until the terminus stalls in shallower water or at a constriction in the fjord (e.g., Åkesson et al., 2018; Amundson & Carroll, 2018; Catania et al., 2018; Mercer, 1961; Nolan et al., 1995; Post, 1975). Over time, positive mass balance in combination with MB growth can lead to glacier growth and readvance, potentially asynchronous with regional trends (e.g., Taku Glacier: Pelto et al., 2008; Post & Motyka, 1995; Hubbard Glacier: Barclay et al., 2001; Trabant et al., 2003).

While morainal bank complexes are widely recognized in theory and in models as stabilizing features for tidewater glacier advance (e.g., Brinkerhoff et al., 2017; Post, 1975), few direct observations of this process exist. Hubbard and Taku glaciers in southeast Alaska are perhaps two of the best examples, where studies within the past two decades have provided rare insights into coupled morainal bank and terminus advance (Goff et al., 2012; Motyka et al., 2006; Nolan et al., 1995; Post & Motyka, 1995; Stearns et al., 2015). A few additional studies have documented interannual moraine growth using repeated bathymetric surveys (Hunter et al., 1996b; Kehrl et al., 2011).

The scarcity of direct observations of MB-facilitated advance may be partly attributed to the seemingly irreversible retreat of many temperate and subpolar glaciers in the past decades to centuries—in other words, numerous glaciers have been progressively retreating without making any readvance (e.g., Columbia Glacier, Post et al., 2011; LeConte Glacier, Post & Motyka, 1995). Thus, at this point in Earth's climate history, it may be more useful to consider the role of morainal banks in delaying retreat, rather than providing a foundation for readvance.

The environmental thresholds for glacier readvance, prolonged stabilization, or onset of rapid retreat are also poorly constrained, but a better understanding of sedimentary processes and feedbacks at the grounding line may help improve future models of glacier retreat (Oerlemans & Nick, 2006; Powell, 1991; Stearns et al., 2015). In temperate and subpolar systems, glacial sediment delivery and reworking can be dynamic on time scales of less than a year, as evidenced by seasonal cycles of advance and retreat (Burton et al., 2016; McNabb & Hock, 2014; O'Neel et al., 2003; Ritchie et al., 2008; Stearns et al., 2015) and by the diurnal, seasonal, and annual variability in sediment delivery rates (Cowan et al., 1988, 1999; Koppes et al., 2010). Thus, in order to better constrain dynamics of morainal banks and potential feedbacks for glacier stabilization (whether for readvance or a delayed retreat), high-temporal resolution of moraine growth and terminus dynamics are needed.

Here we focus on LeConte Glacier in southeast Alaska, which experienced a rapid retreat from an existing morainal bank in 1994–1999, and then stalled at a constriction in the fjord and constructed a new MB between 2000 and 2016. Beginning in 2016, summertime terminus positions became increasingly retracted behind this MB, exposing another fjord basin. Here we use detailed bathymetric and terminus position data collected in 1999–2000 and 2016–2018 to evaluate the growth, morphology, and sedimentary processes associated with MB evolution during this stillstand. Understanding mechanisms of moraine growth provides a needed context for future models aimed at quantifying how grounding-line sediment dynamics may impact glacier stability and modulate retreat over time scales of seasons to decades.

2. Regional Setting

LeConte Glacier (in Tlingit, Xeitl Sít') is the southernmost tidewater glacier in the northern hemisphere. The glacier is 40 km long, covers 480 km^2, and drains from the 5,800-km^2 Stikine Icefield into LeConte Bay (in Tlingit, Xeitl Geeyi') (Figure 1; Kienholz et al., 2015; Melkonian et al., 2016). The fjord eroded by the glacier is ~18 km long and 1–2 km wide with several subbasins of ~130- to 315-m depth separated by sills and/or moraines (Motyka et al., 1998, 2003) and is carved into a granodiorite batholith and relatively

erosion-resistant tonalite (Brew & Friedman, 2002). Here we use the term "sill" to refer to shallow seafloor features such as local bedrock protrusions or moraines deposited during past glacier stillstands (Catania et al., 2018). The Little Ice Age (LIA) moraine near the entrance (Figure 1) was last occupied in ~1780 CE (Post & Motyka, 1995; Viens, 2001). Though LeConte Glacier has undergone periods of rapid retreat characteristic of tidewater glaciers, its retreat has generally been slower than other Alaskan glaciers, owing to its relatively large accumulation area and tendency to become pinned at constrictions in the fjord (Post & Motyka, 1995).

Between 1962 and 1994, the terminus of LeConte Glacier was located ~2 km down-fjord of the present terminus location (Figures 1 and 2). Between 1994 and 1999, the terminus thinned >125 m and rapidly retreated to a new pinning point near where the glacier makes a >90° turn (Figure 1; Arendt et al., 2002; O'Neel et al., 2001, 2003). Since 2000, the glacier terminus has been relatively stable, with seasonal oscillations of up to 300 m (Figures 2 and 3; McNabb & Hock, 2014), as is characteristic of temperate tidewater glaciers (Fischer & Powell, 1998; Powell, 1990). The annual ice flux is ~1 Gt a^{-1}, one of the highest rates among Alaska glaciers (McNabb et al., 2015). Ice flow speeds are ~14–27 m day^{-1} near the terminus (Amundson et al., 2020; Melkonian et al., 2016; O'Neel et al., 2001), with submarine melt rates of ~1–16 m day^{-1} (Jackson et al., 2020; Motyka et al., 2003, 2013; Sutherland et al., 2019).

3. Methods

3.1. Bathymetric Surveys

Bathymetric data were collected in August 1999 and September 2000 using a Furuno 528L fathometer and Trimble Pro XRS GPS receiver and data logger (Hunter & Motyka, unpublished data). Position data were of submeter accuracy, differentially postprocessed with base station data collected for the U.S. Forest Service. The GPS data were standardized to NAD83 UTM Zone 8 coordinates in ArcView. Sounding data were referenced to mean lower low water (MLLW) and postprocessed for tidal corrections using 6-min tidal data from Ketchikan, AK (National Oceanic and Atmospheric Administration [NOAA] CO-OPS Station 9450460) together with tidal delay corrections of +25 min for high water times and +30 min for low water times, and a tidal amplification factor of 1.035 (S. Lyles & L. Hunter, personal communication, 2000). Data were converted from NAD83 to WGS84 UTM Zone 8 using an x offset of −1.2 m and y offset of +0.46 m and were converted from MLLW to mean sea level (MSL) by adding 1.99 m, based on a measured offset from a pressure sensor deployed on a mooring in the fjord during 2016–2018 (Jackson et al., 2020). Converted bathymetric data were then gridded at 20-m resolution using mbgrid in MBsystem (Caress et al., 2018). A Gaussian weighted mean was used for the gridding algorithm, and a spline interpolation was performed to fill gaps of five grid cells or less.

The fjord bathymetry was resurveyed in August 2016 using a Reson SeaBat 7111 multibeam echosounder and Applanix POS/MV 320 WaveMaster, and in May 2017 and September 2018 using a Reson SeaBat T50-P multibeam system. In each case, the multibeam sensor was mounted on a pole at 15° from vertical, in order to capture both the ice face and the seafloor (see Sutherland et al., 2019). Data were corrected for tides and the speed of sound using in situ conductivity/temperature/depth (CTD) profiles and pressure data from a mooring deployed near the glacier (e.g., Jackson et al., 2020). Horizontal position data were obtained from two Trimble 540AP Global Navigation Satellite Systems (GNSS) receivers mounted fore and aft on the survey vessel or from a Hemisphere R330 GNSS receiver (with Hemisphere A42 Antenna), referenced to the WGS84 UTM Zone 8 coordinate system. Raw point clouds were initially cleaned in Caris HIPS and SIPS software to remove spurious datapoints. Point clouds from a subset of multibeam passes that exhibited minimal interference from waves or ship motion were then combined in CloudCompare (http://www.danielgm.net/cc/) and manually cleaned of outliers and ice-face points. These combined point clouds were then gridded in MBsystem (see above), with grid resolutions of 4 m for August 2016, 2 m for May 2017, and 2 m for September 2018 and search radius of three grid cells (instead of five as for the older data) for interpolating across data gaps. May and September point clouds were denser and thus gridded at a finer resolution. Data from August 2016 were also regridded at 20-m resolution (with a search radius of five cells for interpolating across data gaps) for comparison to the older 1999/2000 survey data.

Estimates of accumulation rates and volume changes between surveys were obtained by differencing the 1999/2000 and August 2016 data gridded at 20 m and by differencing the May 2017 and September 2018

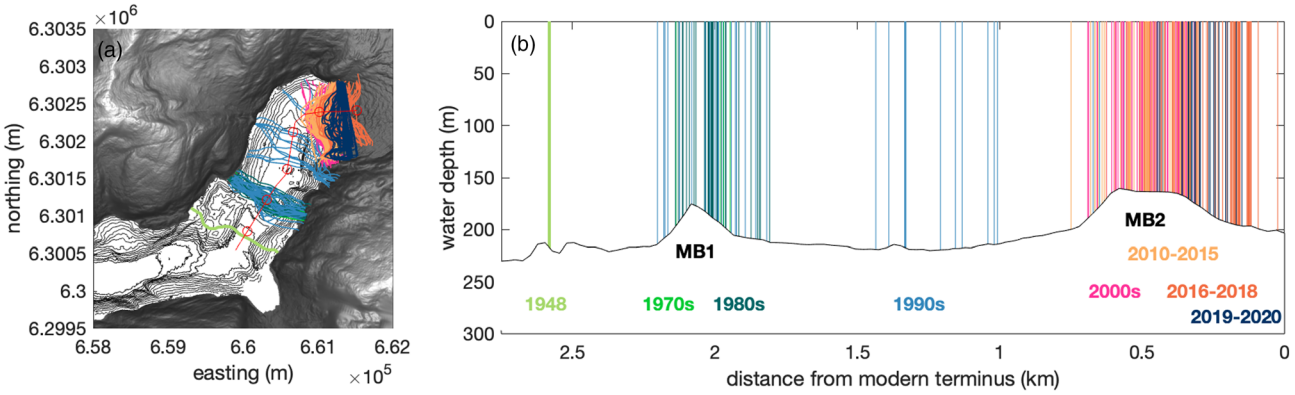

Figure 2. Glacier terminus positions since 1948. (a) Map view, with 2016 bathymetry shown for reference. The red line denotes the reference transect used to the determine along-fjord distance for each terminus location; increments of 0.5 km are noted. The transect begins approximately at the location of the 2016 terminus. (b) Profile view from the red line in (a), illustrating the glacier stillstands at the locations of the two moraines present in 2016 (see also Figure 3). Termini data through 2012 are from McNabb and Hock (2014). Data for 2013–2019 were picked from Landsat Imagery, available through USGS (at https://earthexplorer.usgs.gov/).

data gridded at 2 m. Estimates of errors between the 1999/2000 and August 2016 surveys were difficult to obtain because the highest density of data points from 1999/2000 occurred within the region of greatest sediment accumulation, leaving few regions of constant seabed elevation (i.e., competent bedrock surfaces) for comparison between surveys. Thus, elevation errors were computed for each survey individually, and the largest error was used to determine an error for the accumulation-rate estimate. This approach is detailed in section S2 in the supporting information (see also Schimel et al., 2015). A similar approach was also used to determine elevation and accumulation-rate errors for the modern surveys and is presented in section S2 and Figure S7.

Grounding-line locations were extracted from 19 terminus multibeam scans from August 2016, 9 scans from May 2017, and 13 scans from September 2018 in order to evaluate the horizontal and vertical change in the grounding line. To determine the grounding-line location from each scan, data from the point clouds were subsampled along ice-normal transects spaced 10 m apart with 50% overlap (August 2016), 6 m apart with 0% overlap (May 2017), and 5 m apart with 0% overlap (September 2018). Different spacings and overlap were used because the density of points improved with each survey. The grounding-line location was then manually picked from each profile of the ice face/fjord floor based on any break in continuity of the surface or an obvious transition from ice to seafloor.

3.2. Sediment Samples and Subbottom Profiles

Seabed grab samples were collected from 16 sites and analyzed for grain-size distributions. Subsamples of <2 g were processed through a Beckman-Coulter LS 13320 laser particle sizer at the Oregon State University core lab. Median grain-size values (d_{50}) were computed graphically and data were binned into whole-phi increments. Additional details are given in section S3. More than 45 km of CHIRP subbottom sonar profiles were collected; additional details are given in section S4.

3.3. Suspended-Sediment Data

Profiles of turbidity and salinity were collected along transects spanning ~1 km across fjord at MB1 (Figure 1), in conjunction with acoustic Doppler current profiler (ADCP) measurements. Multiple transects were completed from a small vessel during each survey, providing a view of sediment concentrations and velocity spanning daily fluctuations in meltwater discharge. Turbidity data were calibrated to suspended-sediment concentrations (SSCs) using water samples collected and filtered in the field. The SSC data were then used to calibrate the ADCP backscatter data to obtain estimates of down-fjord sediment flux. Due to the blanking distance and range of the 600-kHz ADCP, fluxes were computed for the upper 5–55 m of the water column. Details of these methods and calculations are given in section S1 and Figures S1–S4.

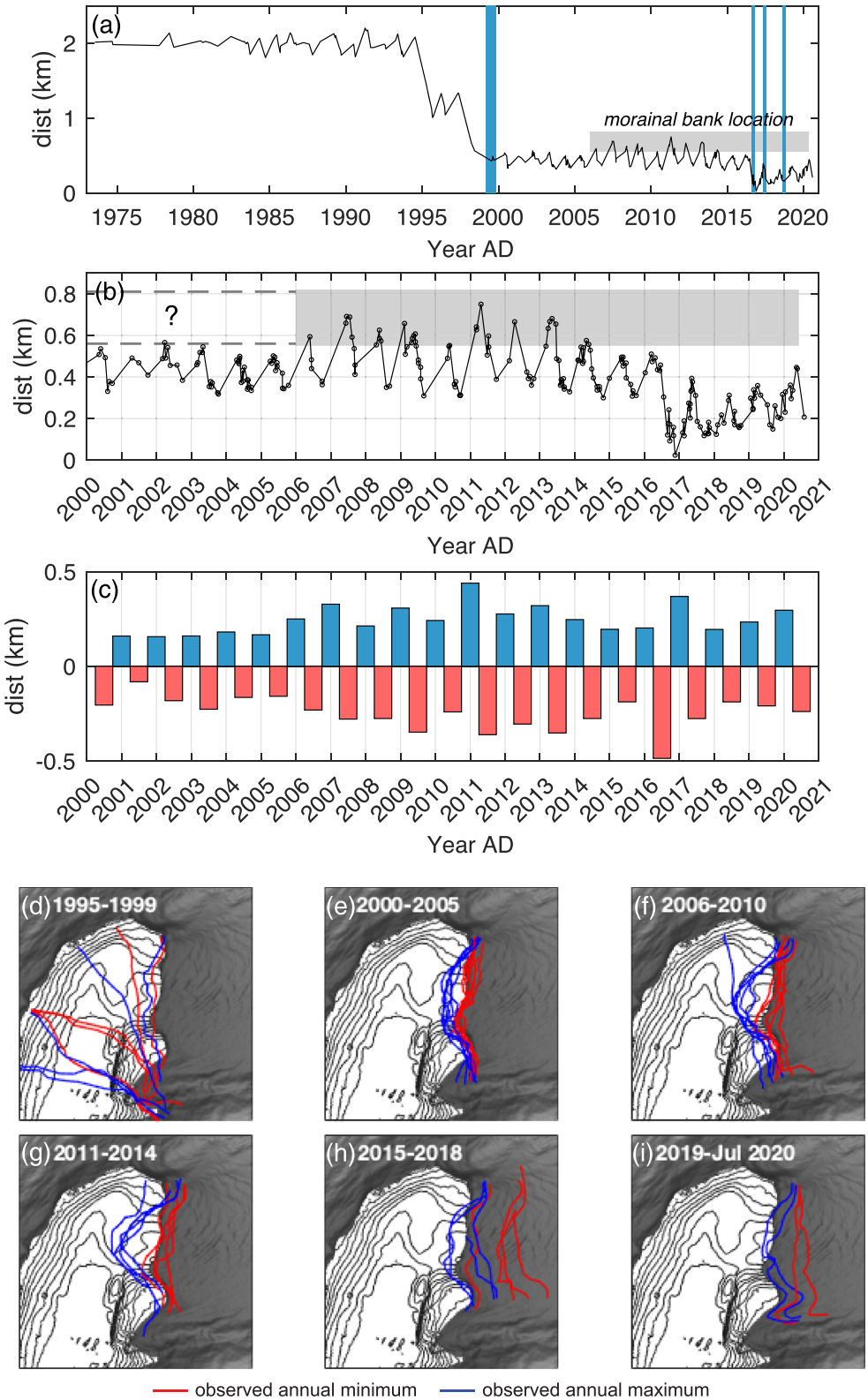

Figure 3. Time series of terminus change. (a) Along-fjord location of terminus, relative to modern reference point. The location of the modern terminal moraine is shown in gray, and times of multibeam surveys are noted in blue. (b) Detail of terminus positions since 2000. (c) Maximum advance and retreat distances for each year since 2000. See note in Figure 2 for data source. (d–i) Maximum and minimum seasonal terminus locations from available imagery for intervals between 1995 and 2020.

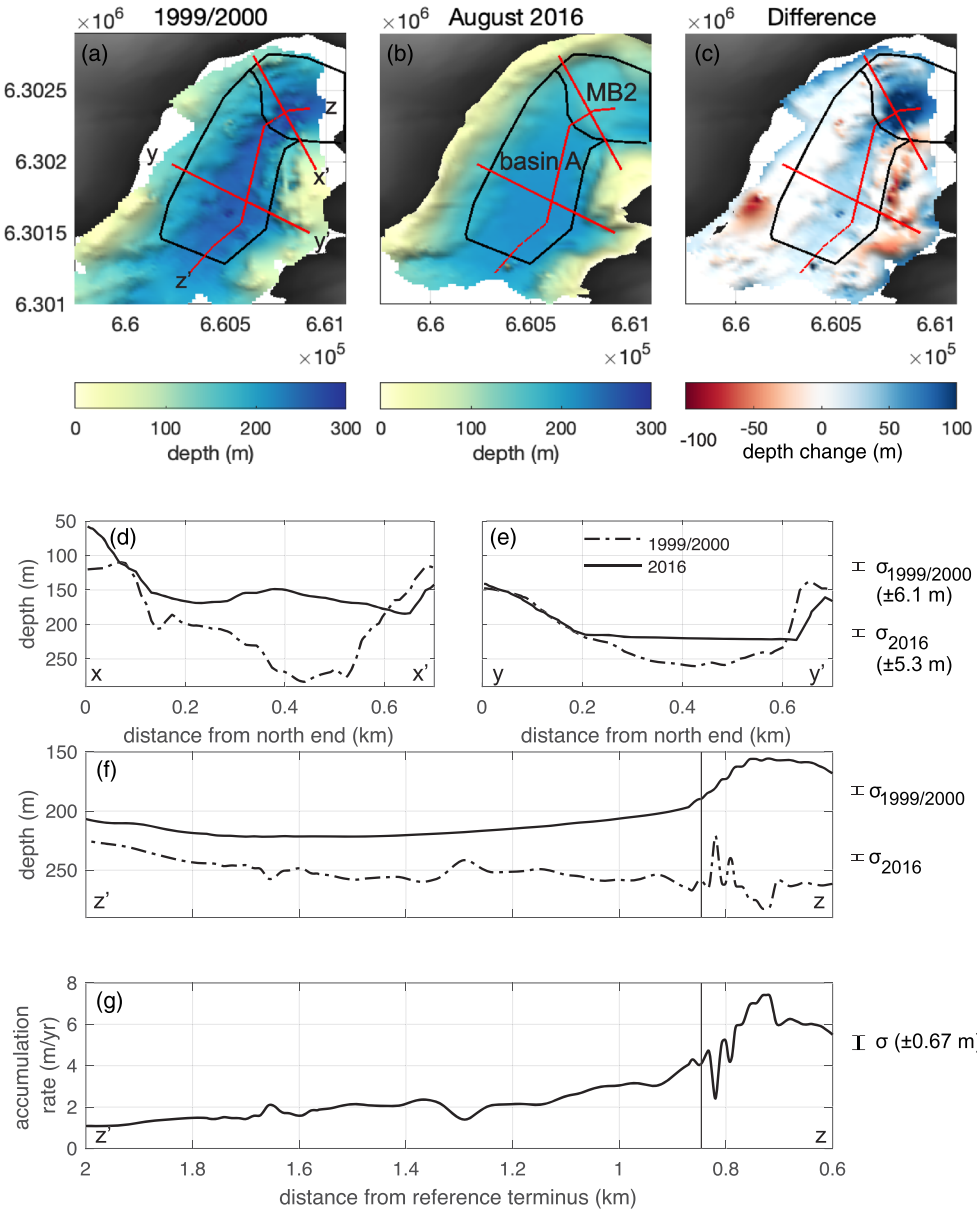

Figure 4. Change in bathymetry between 1999/2000 and 2016. (a) The 1999/2000 bathymetry. (b) August 2016 bathymetry. (c) Elevation difference (B−A). Outlines in (a)–(c) denote regions used for volume calculations (see text). (d) Ice-proximal cross-fjord transect. (e) Ice-distal cross-fjord transect. (f) Along-fjord transect. (g) Mean annual accumulation rate for transect (f) based on elevation change and 17-year time scale. Vertical lines in (f) and (g) denote boundary between morainal bank and basin, as defined for sediment-volume calculations. The distance from terminus is relative to the September 2016 location.

4. Results

4.1. Terminus Changes and Morainal Bank Growth, 1999 to Present

Following rapid retreat from 1994 to 1999, the terminus reached a relative stillstand at its present location where the fjord makes a sharp turn (Figures 1–3). The terminus position has since fluctuated a few hundred meters each season (Figures 3a–3c), with increasing variability in terminus shape and position through time. Between 2000 and 2005, seasonal fluctuations were ~200 m (Figures 3b and 3c), and the wintertime terminus shapes (in plan view) were slightly convex down-fjord (Figure 3e). Between 2006 and 2010, seasonal fluctuations increased to ~200–400 m (Figures 3b and 3c), and the wintertime terminus shape became more convex

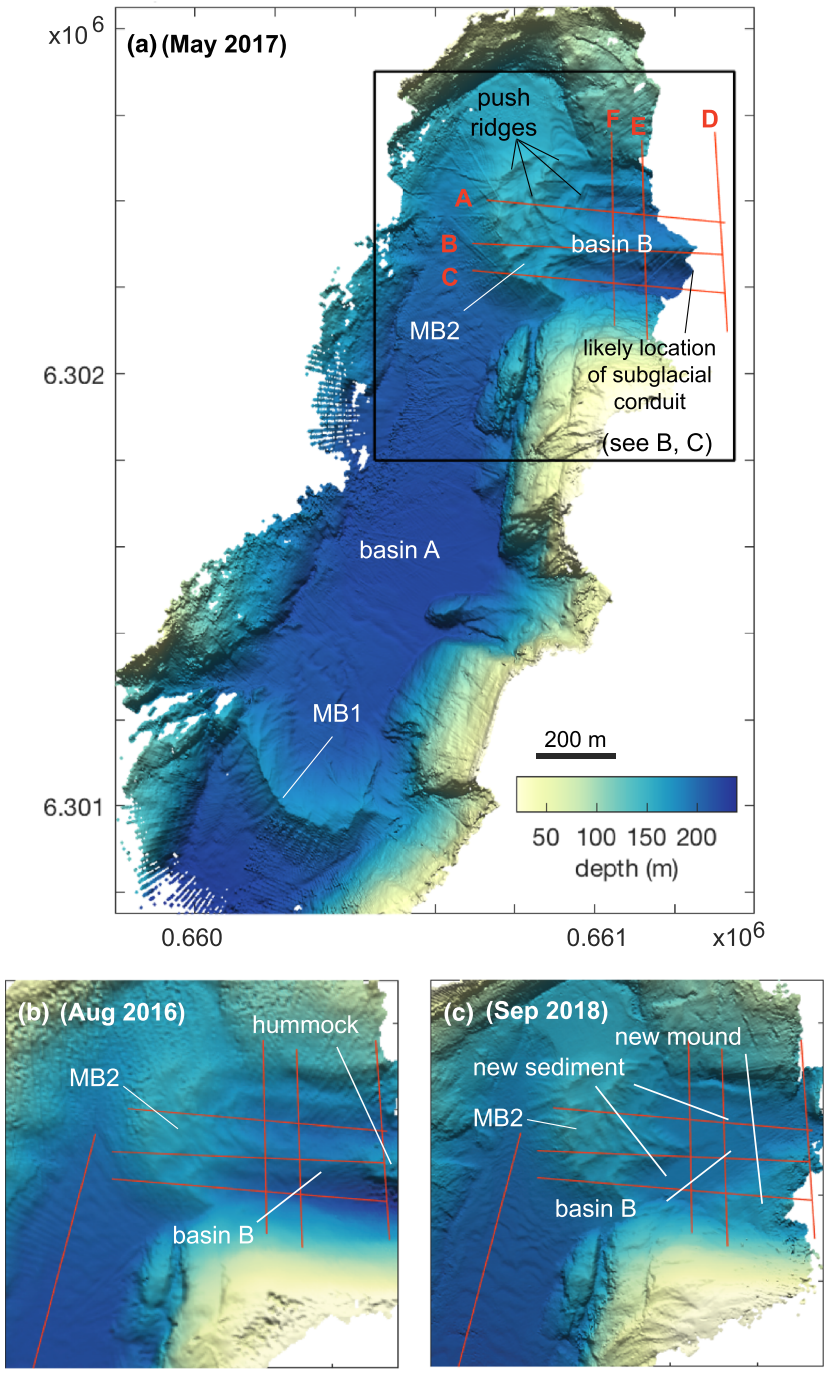

Figure 5. Bathymetry of the inner basin and morainal bank complex, 2016–2018. (a) May 2017 survey, showing the entire inner basin. (b) Detail of MB2, August 2016. (c) Detail of MB2 with new infill in channels, September 2018. (d) Profile of north channel. (e) Profile of medial ridge. (f) Profile of south channel. (g) Cross-fjord profile adjacent to terminus. (h) Cross-fjord profile highlighting new mound in south channel in 2018. (i) Cross-fjord profile highlighting flat infill of both channels in 2018. Transects in red are shown in detail in Figure 6.

(Figure 3f). Between 2011 and 2014, the seasonal changes reached a maximum of ~450 m (Figures 3b and 3c), and the terminus reached its maximum extent corresponding to the crest of the present moraine (Figure 3g). A substantial retreat of ~500 m in 2016 (Figures 3b and 3c) was followed by modest wintertime maxima, but by 2020 the wintertime terminus had readvanced to vicinity of the moraine crest (Figure 3h).

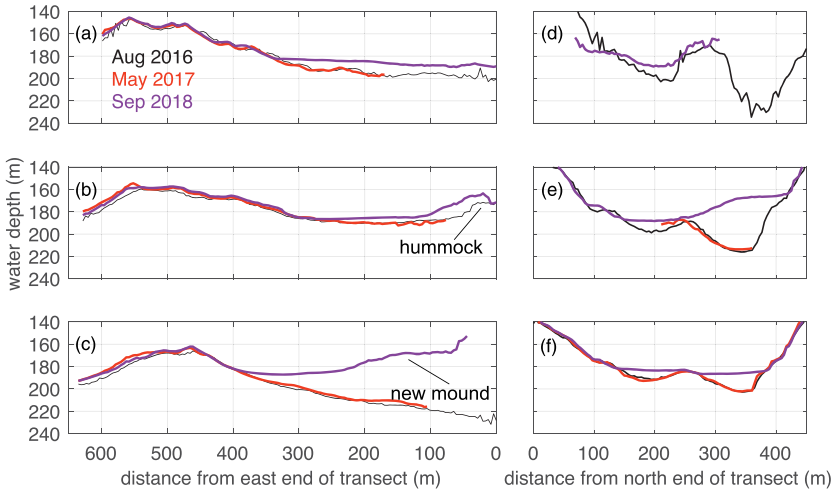

Figure 6. Bathymetry of the inner basin and morainal bank complex, 2016–2018 (transects accompany Figure 5a). (a) Profile of north channel. (b) Profile of medial ridge. (c) Profile of south channel. (d) Cross-fjord profile adjacent to terminus. (e) Cross-fjord profile highlighting new mound in south channel in 2018. (f) Cross-fjord profile highlighting flat infill of both channels in 2018.

The rapid retreat in the late 1990s left a terminal moraine formed between 1962 and 1994 (MB1, Figures 1 and 2) stranded ~2 km from the present-day terminus. The U-shaped basin behind this moraine (Basin A, Figures 1 and 5) was ~240–260 m deep in 1999/2000, with a maximum depth of 280 m near the terminus (Figure 4). At the time of its opening, Basin A was the shallowest and smallest of the subbasins behind the LIA moraine (Figure 1).

Between 1999/2000 and 2016, a new morainal bank complex grew in the deepest part of Basin A, reaching heights of up to 140 m above the 1999/2000 seabed (this feature is denoted MB2, Figure 4) and ~150 m below sea level. The crest of MB2 is more than 100 m wide (along-fjord) and is wrinkled by a series of small ridges ~3–8 m high (Figures 5 and 6). These features are well defined in the high-resolution May 2017 and September 2018 data and are relatively static between the two surveys. The ice-distal face of MB2 slopes toward the basin floor at 14–26°. The ice-proximal face slopes toward the glacier at 6–22°.

The total volume of MB2 is estimated to be $93 \times 10^5 \pm 59 \times 10^5$ m^3, based on the difference between the 2016 and 1999/2000 bathymetric grids (region "MB2", Figure 4b). To account for void spaces in the sediment (expressed as porosity), the total mapped volume has been adjusted to obtain the net volume of sediment (excluding voids). Truffer et al. (1999) measured a porosity of 40% for subglacial till at Black Rapids Glacier. Porosities of tills in Antarctica have been estimated at 40% during deformation and 30% postdeformation (e.g., Alley et al., 1987). If we reduce the estimated moraine volume by a porosity of 35%, we obtain an estimated sediment volume of $60 \times 10^5 \pm 38 \times 10^5$ m^3, representing a mean annual flux of $3.5 \times 10^5 \pm 2.2 \times 10^5$ m^3 a^{-1} during the 17-year interval (Table 1).

The morainal bank and the small ridges on the crest remained relatively static in terms of location, shape, and height between 2016 and 2018. In contrast, the front (distal) side lost a few meters of sediment while the seaward basin accumulated sediment (Figure 7a). The platform at the north end of MB2 experienced several meters of erosion, which continued along a chute toward the basin floor (Figure 7a). A transect through this zone (S-S′, Figures 7a–7c) shows a series of small hummocks stepping down the chute and mean seafloor slopes of ~2–4°. In May 2017 the hummocks were 0.65 m high (on average) with a mean spacing of 26 m, and in September 2018 they were 0.98 m high with mean spacing of 30 m, although the change in height is less than the uncertainty.

4.2. Sediment Deposition and Reworking in Basin A

Over the past 17 years, Basin A has filled with $84 \times 10^5 \pm 19 \times 10^5$ m^3 of material, based on the difference between the 1999/2000 and 2016 bathymetric grids within the area outlined in Figure 4b. (Note that this area falls short of MB1, meaning the basin volume is slightly underestimated.) If we again assume a porosity of

Table 1
Summary of Sediment Flux (Q_s) and Accumulation Rate (S) Estimates, Suspended Sediment Flux Beyond the Basins, and Total Sediment Flux

Period	Q_s[a], MB2[b] ($m^3\ a^{-1}$)	Q_s, Basin A[b] ($m^3\ a^{-1}$)	S ($m\ a^{-1}$)	Suspended flux ($m^3\ a^{-1}$)	Total estimated flux ($m^3\ a^{-1}$)
1999/2000–2016	$3.5 \times 10^5 \pm 2.2 \times 10^5$	$3.2 \times 10^5 \pm 0.71 \times 10^5$	$1.1–4.0 \pm 0.67$	N/A	N/A
2016–2017	N/A	N/A	$0–4.0 \pm 10$	N/A	N/A
2017–2018	$3.2 \times 10^5 \pm 0.068 \times 10^5$	$2.7 \times 10^5 \pm 0.068 \times 10^5$	$0–2.7 \pm 6.5$	0.91×10^5	6.8×10^5

[a]Q_s includes sediment deposited in Basin B between the 2017 and 2018 surveys. [b]Moraine and basin fluxes are based on assumed porosities of 30–40%.

35%, we obtain an estimated sediment volume of $55 \times 10^5 \pm 12 \times 10^5$ m^3 and an annual flux of $3.2 \times 10^5 \pm 0.71 \times 10^5$ $m^3\ a^{-1}$. On an interannual time scale (May 2017 to September 2018), the total volume of material deposited in Basin A was $5.6 \times 10^5 \pm 0.14 \times 10^5$ m^3, representing a mean annual flux of $2.7 \times 10^5 \pm 0.068 \times 10^5$ $m^3\ a^{-1}$ (Table 1).

Along the fjord axis (Figure 8), linear sediment accumulation rates were $1.1–4.0 \pm 0.67$ m a^{-1} on a decadal time scale (1999/2000–2017) and $0–4.0 \pm 10$ m a^{-1} on an interannual time scale (periods between 2016, 2017, and 2018 surveys; Table 1 and Figure 8).

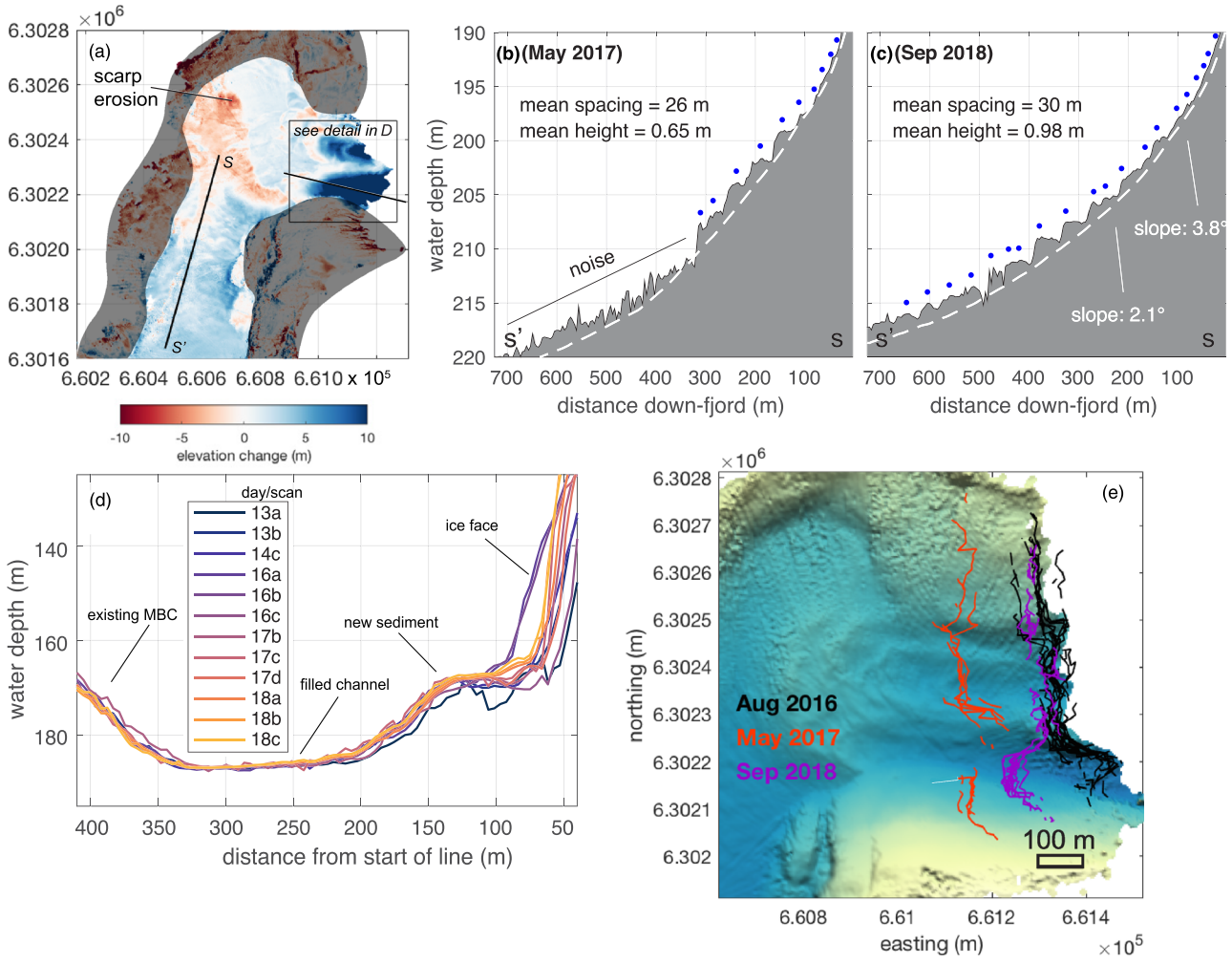

Figure 7. Evidence of sediment reworking and redistribution over interannual time scales. (a) Difference between September 2018 and May 2017 bathymetry. Blue denotes deposition and red denotes erosion. (b) Profile along Transect S-S′ (in a) from May 2017, highlighting bedforms. Blue dots are locations of bedform crests. (c) Profile of Transect S-S′ from September 2018. (d) Detail of bathymetry difference near the terminus, for dates given in September 2018. Up to 46 m of sediment was deposited in 16 months. (e) Variability in grounding-line location for each modern survey (background bathymetry is from August 2016).

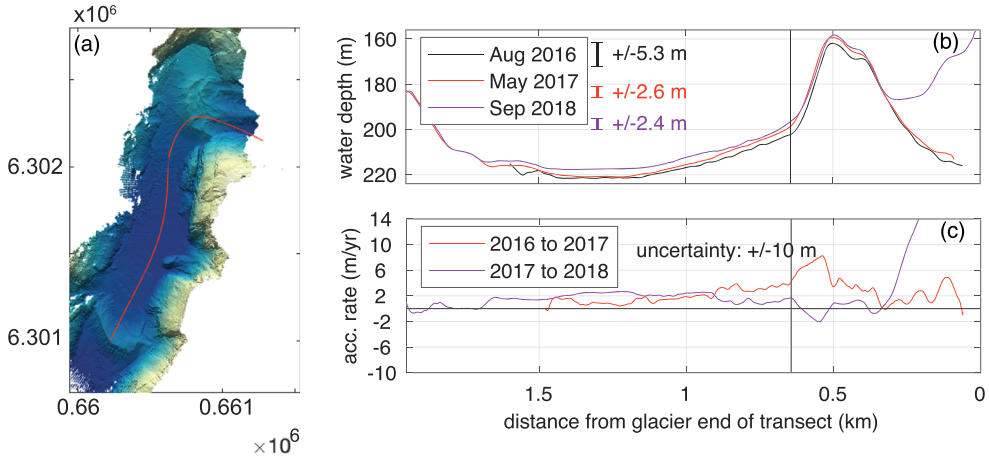

Figure 8. Interannual accumulation rates for an along-fjord transect. (a) Transect, superimposed on May 2017 bathymetry. (Color scale is the same as in Figure 5.) (b) Bed elevation for the three recent surveys, with uncertainty for each noted. (c) Accumulation rates between surveys, converted to m a^{-1}, based on differenced bathymetry. Uncertainty of ±10 m is noted. High rates (>10 m a^{-1}) adjacent to the ice represent the sediment deposited between May 2017 and September 2018. The vertical line in (b) and (c) denotes the end of the morainal bank and start of basin fill. Note that the reference transect differs from Figures 2–4 in order to highlight the new ice-proximal sediment mound in the south channel.

Sediments at the center of Basin A are generally flat lying and acoustically opaque (Figures S9b–S9d). For context, sediments in the basin seaward of MB1 exhibit at least tens of meters of parallel strata at the seabed surface (Figure S9d), and sediments seaward of the LIA moraine exhibit >100 m of similarly acoustically stratified deposits (Figure S9e).

Surface grab samples were collected in 2017 in the center of Basin A and near MB1. Samples yielded mixed sands and muds that were generally unimodal but poorly sorted, with median grain sizes (d_{50}) of 6.5 to 2.7 phi (11 to 157 μm), that is, fine silt to fine sand (Figure S8). Many grab samples arrived relatively undisturbed and exhibited a soft, muddy surface layer above sandy sediment.

4.3. Sediment Deposition and Reworking in Basin B

A new subbasin (Basin "B", Figures 1 and 5) is emerging behind MB2 and is characterized by two along-fjord-trending channels separated by a ridge (Figures 5 and 8). The north and south channels have maximum depths of ~200 and ~230 m, respectively. The ridge is ~185 m deep. A 10-m-high hummock appeared on top of the ridge adjacent to the ice in August 2016 (Figure 6b).

Summertime retreat of the terminus in 2016 and 2017 exposed Basin B (Figures 5 and 6). By 2018, this had filled with flat-lying sediments, as well as a new ~40-m-high mound of sediment adjacent to a substantially overcut section of the ice face (Figures 5c, 6c, 6e, 7a, 7d, and 8b). This mound was mapped using the multibeam system one to three times per day during daylight hours between 13 and 18 September 2018; the profiles indicate a forward motion of the mound by more than 20 m in 5 days and substantial changes in terminus geometry (Figure 7d). In fact, during all three bathymetric surveys (August 2016, May 2017, and September 2018) the location of the terminus varied over distances of tens of meters on daily time scales (Figure 7e).

The net volume of new material deposited in Basin B and on MB2 between May 2017 and September 2018 was $6.6 \times 10^5 \pm 0.14 \times 10^5$ m^3. This is equivalent to a mean annual sediment flux of $3.2 \times 10^5 \pm 0.068 \times 10^5$ m^3 a^{-1} (assuming a porosity of 35% as noted above), similar to the value derived for the longer 1999/2000–2016 time period.

4.4. Total Glacial Sediment Flux

Suspended-sediment bypass of Basins A and B was estimated for three surveys in 2017 (May, July, and September) using calibrated ADCP measurements from across-fjord transects (Figures S4a and S4b and

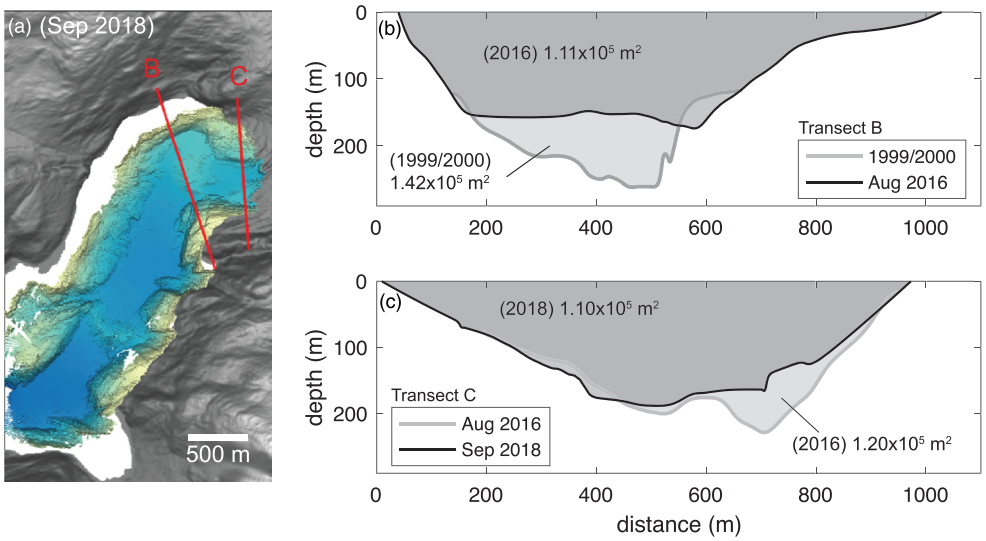

Figure 9. Changes in cross-sectional area of fjord. (a) Transect locations. (b) Decadal-scale area change (i.e., change in exposure of terminus) between 1999/2000 and 2016, due to the growth of the morainal bank at Transect B. (c) Interannual area change between 2016 and 2018, due to the deposition of new sediment at Transect C. Distances start at the north ends of transects.

sections 3.3 and S1). Estimated down-fjord sediment fluxes at 5- to 55-m water depth ranged from −1.8 to 3.4 kg s^{-1} in May, 5.2 to 38 kg s^{-1} in July, and 0.31 to 53 kg s^{-1} in September (Figures S4b–S4f). Positive fluxes are down-fjord. The greatest fluxes occurred in the near-surface plume, which was typically concentrated at <30-m water depth and varied in location between the north and south sides of the fjord (see also Jackson et al., 2020; Kienholz et al., 2019). SSCs in the plume between the MB1 and MB2 (Figure 1) were generally <30 mg/L. If we make a rough estimate that the mean sediment flux was ~23 kg/s for the summer months of June–September, representing a total of 122 days, we estimate a conservative suspended-sediment flux of 9.1×10^4 m^3 a^{-1} beyond Basin B. This value neglects sediment discharge at 0–5 and >55 m in the water column and neglects sediment discharge occurring during nonsummer months. Because of these important unknowns, an uncertainty has not been computed for the estimated suspended flux.

Because direct measurements of glacial sediment delivery are difficult to make, the summation of sediment volumes deposited near the glacier and suspend-sediment bypass in the meltwater plume are sometimes used as a proxy. Between 2017 and 2018, Q_s (sediment flux) to MB2 (including Basin B) was $3.2 \times 10^5 \pm 0.068 \times 10^5$ m^3 a^{-1}, and Q_s to Basin A was $2.7 \times 10^5 \pm 0.068 \times 10^5$ m^3 a^{-1}. The estimated suspended flux past Basin A was 0.91×10^5 m^3 a^{-1}, and thus, the total estimated glacial sediment flux was 6.8×10^5 m^3 a^{-1}. Because of the limited scope of suspended-sediment measurements, this value is likely underestimated, and no uncertainty has been provided (see above).

4.5. Impacts of Sediment Delivery on Terminus Exposure

Moraine growth and seasonal fluctuations of the terminus position changed the area of the terminus exposed to saltwater over seasonal to decadal time scales. In 1999/2000, the cross-sectional area near the terminus was 1.42×10^5 m^2 (Figures 9a and 9b). By 2016, MB2 had reduced this area to 1.11×10^5 m^2, a change of 22%. Between 2016 and 2018, sediment deposition at the grounding line reduced the fjord area proximal to the face from 1.20×10^5 m^2 in August 2016 to 1.10×10^5 m^2 in September 2018, a change of 10% (Figure 9c).

5. Discussion

Repeated bathymetric measurements adjacent to the LeConte glacier terminus offer a rare view into the evolution of a morainal bank on interannual time scales during a stillstand, starting immediately after a rapid glacier retreat. These measurements of short-timescale delivery and reworking are useful for interpreting

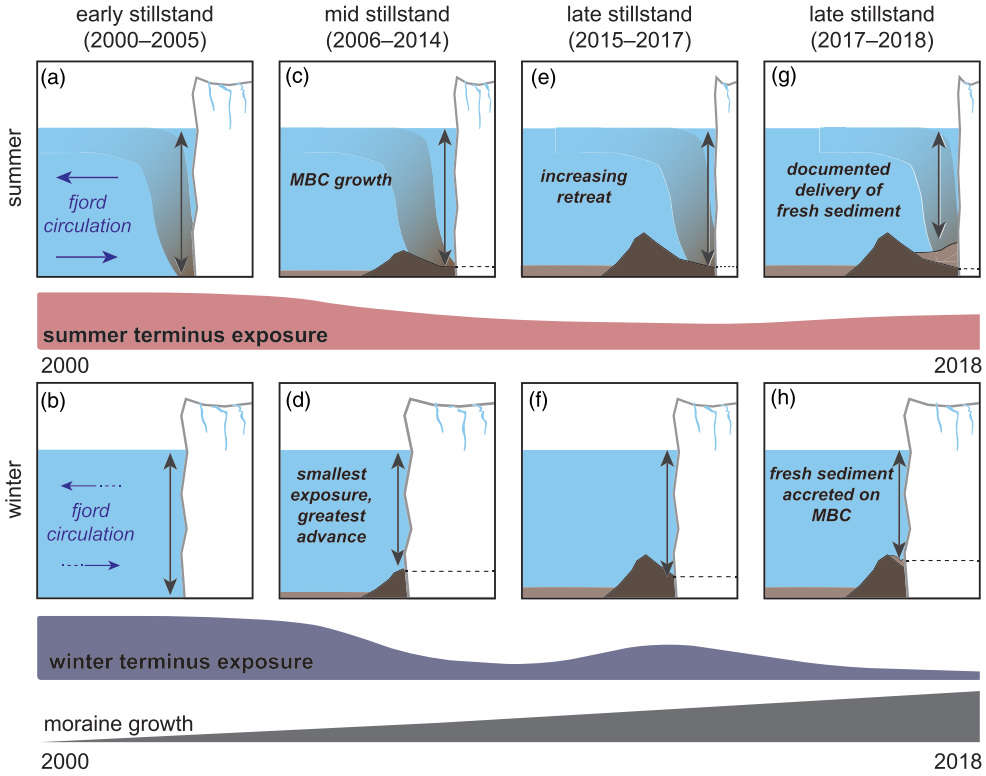

Figure 10. Changes in terminus area during tidewater-glacier stillstand and morainal bank evolution. (a) Delivery of sediment to newly opened basin (a). (b) Winter advance. (c) Morainal bank complex growth during summers. (d) Winter terminus advances to crest of moraine. (e) Summer terminus positions are increasingly retracted. (f) Winter terminus positions are less advanced than in past years. (g) In 2017–2018, fresh delivery of sediment was documented. (h) Based on satellite-derived termini positions, fresh sediment from (g) was likely accreted onto moraine. The summer and winter terminus exposures gradually decreased as the morainal bank complex grew (winter exposures were affected to a greater degree). Fjord circulation is generally stratified as noted in (a) and (b), and more variable in winter than in summer (see Kienholz et al., 2019).

relict fjord deposits, as well as feedbacks on terminus dynamics that are needed in models of glacier retreat. Here we discuss sedimentation processes (sections 5.1 and 5.2) and implications for glacier dynamics (sections 5.3–5.5).

5.1. Sediment Dynamics and Moraine Growth

The modern morainal bank complex (MB2) constructed by LeConte Glacier since 1999 (during its stillstand at a lateral pinning point) exhibits features characteristic of modern and relict moraines in diverse fjords (e.g., Dowdeswell et al., 2015; Dowdeswell & Vásquez, 2013; Streuff et al., 2018). The moraine composition is inferred to be a mixture of unsorted diamictons and (temporarily) sorted glacifluvial sediments, based on (1) prior studies by Hunter et al. (1996a, 1996b) in Glacier Bay, which found these two sediment facies to be the most common near the grounding line (relative to sediment derived from calve dumping, suspension settling, etc.); (2) the steepness of the bank (14–26°), which is consistent with observations of overconsolidated, unsorted proglacial diamictons with slopes of 6–18° in other systems (Goff et al., 2012; Hoek & Bray, 1981; Larter & Barker, 1989; Seramur et al., 1997); and (3) observations of rapid sediment deposition near the subglacial conduit in 2017–2018 (section 5.2).

Powell (1990) described initial deposition of glacifluvial fjord sediments in grounding-line (ice-contact) fans, which are deformed and reworked (together with diamictons extruded from the base of the glacier) during advances of the terminus to form complex mixtures of sorted, unsorted, and reworked sediments of diverse sizes (Elverhøi et al., 1980). The seasonal variations in terminus position at LeConte suggest that a similar process has been happening since 1999. During each summer melt season, abundant

glacifluvial sediments are delivered to the grounding line while the terminus is retracted and then reworked into MB2 during the winter readvance (Figures 3 and 10). As MB2 grew by this annual cycle of delivery and reworking between 1999 and 2016, it is reasonable to expect changes in the terminus shape (Figures 3d–3i). Tidewater glacier termini are thought to form a seaward bulge in the center where a "bathymetric pinning point" (or bathymetric high) exists (Carr et al., 2014). Between 2000 and 2014, the terminus of LeConte became increasingly more convex (down-fjord), suggesting progressive growth of MB2 and increasing feedbacks on terminus stabilization (Figures 3d–3i and 10; see section 5.4).

In addition to seasonal and interannual changes in terminus shape, the dynamic evolution of MB2 is evident in small-scale ridges on the ice-proximal crest of MB2 (Figures 5a and 5c). These features are consistent with "push ridges" observed in other marine and terrestrial proglacial systems (Bennett, 2001; Boulton et al., 1996; Johnson et al., 2013; Kristensen et al., 2009; Ottesen & Dowdeswell, 2006; Seramur et al., 1997) and are interpreted to be formed by seasonal readvances of the terminus as it progressively bulldozes summertime glacifluvial deposits forward and accretes them onto the moraine (see also Boulton, 1986). Interestingly, the push ridges observed on the crest in 2017 were still present in 2018, consistent with satellite-derived evidence that the terminus did not regain the moraine crest that winter (Figure 3h).

Between 2017 and 2018, the annual flux of sediments to emergent Basin B was $3.2 \times 10^5 \pm 0.068 \times 10^5$ m^3 a^{-1}. These sediments are inferred to represent the typical seasonal influx of glacifluvial sediments, which were then available to be accreted onto MB2 during the following winter. We make this interpretation because (1) this annualized flux is similar to the long-term mean flux for MB2 ($3.5 \times 10^5 \pm 2.2 \times 10^5$ m^3 a^{-1} for 1999/2000–2016) and (2) the sediments formed a mound near the ice, where the meltwater conduit was likely located (see Jackson et al., 2020; Pfirman & Solheim, 1989; Figure 5c). The large accumulation near the supposed conduit is consistent with rapid glacifluvial dumping from the plume at the transition point between inertial and buoyant flow followed by failure and formation of gravity flows into the basin (Pfirman & Solheim, 1989; Powell, 1984; Syvitski, 1989). Similar infilling was not apparent in the August 2016 survey; however, glacifluvial sediment discharge is generally thought to vary year by year according to precipitation patterns, connectivity in a subglacial hydrologic network, and other variables (Cowan & Powell, 1991; Cowan et al., 1988; Overeem et al., 2017). In February 2019, the satellite-derived terminus position was advanced from the September 2018 position, indicating that the sediment deposited in 2017–2018 has likely been disturbed since then (Figure 3i). We also note that the mound of ice-contact sediment appeared to be advancing with the ice front during the September 2018 survey (Figure 7d), which is unsurprising based on conceptual models of glaciers plowing through ice-contact sediment fans (Boulton, 1986; Kuriger et al., 2006).

The repeated bathymetric scans, especially from 2017 and 2018 (when greater spatial resolution was attained), provide evidence of dynamic processes of sediment redistribution. These are commonly inferred from analyses of deposits in other systems after the glacier has retreated from the area. For example, many fjord basins contain flat-lying, parallel sedimentary layers attributed to sediment-gravity flows and plume deposition, which fill and obscure the preexisting basin topography with sands and muds (e.g., Anderson, 1999; Cowan et al., 1996; Love et al., 2016; Streuff et al., 2018; Willems et al., 2011). Gravity flows (downslope movements of negatively buoyant water mixed with high concentrations of sediment) are thought to be generated by direct underflows of extremely turbid glacial effluent or by failures of sediments from the grounding-line fan, once the deposits have become oversteepened—either through rapid deposition of coarse sediments by the outflow plume and/or bulldozing by the terminus (Dowdeswell et al., 2015; Powell, 1984, 1990; Syvitski, 1989; Syvitski et al., 1987). These types of downslope flows can be generated in other environments including lakes and submarine canyons, where they commonly generate a series of sedimentary bedforms (e.g., Fricke et al., 2015; Smith et al., 2005). Between 2017 and 2018, erosion from the upper, ice-distal part of MB2 and deposition downslope (Figure 7a) is consistent with this idea of slope failure and redeposition by gravity flows, especially when coupled with observations of a series of regularly spaced bedforms up to 1 m high (Figures 7b and 7c). The bedforms are analogous to antidunes or cyclic steps associated with gravity flows in lakes or deglaciated fjords (e.g., Clare et al., 2016; Hughes Clarke, 2016; Normandeau et al., 2016).

Downslope of this area, the floor of Basin A is relatively flat (Figure 5a), consistent with observed gravity flow and plume-derived deposits in other fjords (e.g., Anderson, 1999; Cai et al., 1997; Cowan et al., 2010; Willems et al., 2011). The presence of parallel sedimentary layers could not be confirmed because coring

attempts were unsuccessful and the near-surface layers were generally acoustically opaque in the subbottom data (Figure S9)—both of which are unsurprising given the high sand contents of surface grab samples from Basin A (Figure S8). Subbottom data from the outer fjord near the LIA moraine, however, exhibited tens of meters of parallel strata (Figure S9e), suggesting that gravity flow deposits have formed in this fjord in the past.

5.2. Rates of Sediment Flux and Accumulation, and Implications for Glacial Erosion Rates

The sediment fluxes and accumulation rates in LeConte Bay are high relative to most coastal sedimentary environments but are moderate to low relative to other tidewater glacier fjords in southeast Alaska. Apparent linear sediment accumulation rates in Basin A were up to 4.0 m a^{-1} based on the both the 17-year change in elevation and the more recent 16-month change in elevation (Figures 4g and 8c). These rates are of the same scale as rates documented in other tidewater systems of southeast and south central Alaska (e.g., Jaeger & Nittrouer, 1999; Love et al., 2016; Powell & Molnia, 1989). The decay of accumulation rate down-fjord is consistent with progressive settling of plume sediments and limited runout distances of gravity flows seen in other systems (e.g., Boulton, 1990; Curran et al., 2004; Meslard et al., 2018; Powell, 1990; Syvitski, 1989). Relative to fjords outside Alaska (e.g., Antarctica, Boldt et al., 2013; Canada, Smith & Walton, 1980; Eidam et al., 2019; Patagonia, Boldt et al., 2013; Svalbard, Elverhøi et al., 1983), accumulation rates in LeConte Bay tend to be 1–2 orders of magnitude greater.

By combining estimates of sediment flux to MB2 (inclusive of Basin B, for reasons given above) and Basin A with estimates of sediment bypassing in the plume, we estimate a total sediment flux from the glacier of 6.8×10^5 m^3 a^{-1}. This is likely a conservative value, because the seaward end of Basin A was excluded (due to limited data coverage) and we used sparse data on suspended-sediment fluxes bypassing the basin —though our estimate of 0.91×10^5 m^3 a^{-1} of suspended-sediment bypass is of the same order of magnitude as an estimate made by L. Hunter (unpublished data) of 0.2×10^5 m^3 a^{-1} in the late 1990s.

Hunter (unpublished data) estimated a mean catchment erosion rate of ~4 mm a^{-1} for LeConte Glacier, based on estimated sediment accumulation in the Basin A of 3.6×10^6 m^3 a^{-1} between 1998 and 2000. Our updated sediment flux estimate is an order of magnitude smaller, giving an effective erosion rate for LeConte Glacier of ~1.4 mm a^{-1}. Both values are significantly smaller than the 10–100 mm a^{-1} range reported for other southeast Alaska tidewater glaciers (Hallet et al., 1996). We attribute these differences in erosion rates to differences in bedrock. LeConte Glacier erodes a highly competent, erosion-resistant tonalite batholith, while the majority of the other southeast Alaska tidewater glaciers analyzed in the Hallet et al. (1996) data set erode much less competent metamorphic terrain. Thus, not surprisingly, glacier basin bedrock appears to make a significant difference in erosion and sediment yields at tidewater glacier termini. Higher sediment yields from more readily erodible glaciated basins can therefore lead to more rapid development of morainal bank complexes (which can stabilize termini during prolonged standstills) than in granitic basins of comparable area and geometry.

5.3. Pinning Points and Step Change Retreats

Tidewater glacier fjord geometry is known to play a role in stabilizing a retreating terminus, by providing a variety of pinning points—for example, constrictions, sills, and bends—which can impede frontal ablation by reducing the area exposed to melting, reduce calving rates by altering near-terminus stresses, and allow the glacier time to thicken (Åkesson et al., 2018; Amundson & Carroll, 2018; Carr et al., 2014; Catania et al., 2018; Mercer, 1961; Post, 1975). McNabb and Hock (2014) applied the term "step change retreats" to tidewater glacier retreats where constrictions or other factors result in a stillstand of several years or more between periods of rapid retreat. Nearly all retreating tidewater glaciers in Alaska experienced a stillstand and stabilized for some time period at a constriction in their fjord in the past several decades (McNabb & Hock, 2014). Columbia Glacier paused its current retreat at a major sill (1994–1997) and then at a constriction in 2000–2006 (Love et al., 2016). Other stepped retreats have been documented in Greenland (Csatho et al., 2008; Howat & Eddy, 2011; Motyka et al., 2017; Sohn et al., 1998), Patagonia (Holmlund & Fuenzalida, 1995; Koppes et al., 2009; Lastras & Dowdeswell, 2016), and Svalbard (Burton et al., 2016).

At LeConte Glacier, a stillstand occurred between 1942 and 1948 (Mercer, 1961) and likely at other times given the sinuous fjord geometry (Figure 1; Post & Motyka, 1995). In 1962–1994, the glacier stabilized at a constriction where it produced MB1 (Figures 1, 2, and 5a; see also Motyka et al., 1998). The AAR is often

used as an indication of a glacier's health and is equal to the area of the glacier's accumulation zone divided by the total glacier area. A glacier is more likely to advance if it has a high AAR, that is, >0.7 (Post & Motyka, 1995; Trabant et al., 2003). Post and Motyka (1995) reported a robust AAR for LeConte Glacier of ~0.90 for the 1962–1994 time period based on early-fall aerial photo surveillance of snowlines. For comparison, the advancing Hubbard Glacier is reported to have an AAR of 0.95 (Trabant et al., 2003) with a submarine moraine that rises to less 100 m below sea level (Goff et al., 2012; Stearns et al., 2015). The question arises as to why LeConte is retreating while Hubbard is advancing. Part of the answer is that despite LeConte's high AAR, the glacier has experienced significant thinning for decades (Arendt et al., 2002; Larsen et al., 2007), whereas Hubbard Glacier has been gaining mass (Arendt et al., 2002; Larsen et al., 2015). Thus, frontal ablation at LeConte must have balanced and then eventually outpaced ice flux to the terminus in 1994.

A tidewater glacier can only advance by remobilizing and pushing its submarine moraine farther downfjord, for example, ~32 m a^{-1} for Hubbard Glacier (Goff et al., 2012). Thus, it appears that some critical combination of sedimentation, climate change, shoal height and size, ocean conditions, and surface mass balance must occur in order to stimulate tidewater glacier terminus advance. At Hubbard Glacier, sediment flux into Disenchantment Bay is $76.9 \pm 11.54 \times 10^6$ m^3 a^{-1} along the 9-km terminus (Goff et al., 2012; Trusel, 2009) or 8.5×10^6 m^3 a^{-1} per km, 2 orders of magnitude greater than at LeConte Glacier (6.8×10^5 m^3 a^{-1}, Table 1). The comparatively lower rate of erosion and sedimentation at LeConte apparently has limited the growth rate of morainal bank complexes during past standstills to a level below that needed to sufficiently curtail frontal ablation and allow advance. With a warming climate, regional temperatures have risen (McNabb & Hock, 2014), and thinning rates at LeConte Glacier have accelerated (Berthier et al., 2018). However, the terminus has also retreated into an even narrow part of its channel, concentrating sedimentation in a tighter area, setting an interesting competition between a warming climate and sedimentation.

5.4. MB2 and Implications for Glacier Terminus Dynamics

The evolution of MB2 has now significantly modified the bathymetry of the innermost fjord, which in turn affects glacier geometry, terminus dynamics, and fjord circulation. Morainal banks act to stabilize tidewater glacier termini by (1) reducing the area of the glacier exposed to the influences of ocean melting (Figure 10); (2) reducing the buoyancy (and thus calving) of the terminus; and (3) exerting backstress on the glacier (e.g., Meier & Post, 1987; Nick et al., 2007; Powell, 1991; Truffer & Motyka, 2016). In the latter, back pressure exerted by a morainal bank acts to reduce the extensional strain rates commonly found near the termini of tidewater glaciers, helping to limit thinning rates during retreat (e.g., Amundson, 2016; Fischer & Powell, 1998; Stearns et al., 2015). In addition to reducing frontal ablation, morainal banks also modulate inner fjord circulation (e.g., at LeConte Glacier, inflow is restricted to warmer layers while colder, more saline waters are isolated at depth in the basin between MB1 and MB2; Sutherland et al., 2019). At LeConte, the stabilizing influence of MB2 has likely fluctuated over the period of 1999–2018 because the terminus has advanced and retreat varying amounts in each year relative to the morainal bank (Figure 10). Through the continued deposition of new material at the current terminus location, the morainal bank may continue to provide a stabilizing influence; alternatively, if significant summertime retreats like those observed in 2016 (Figure 3) continue to occur, the glacier may begin a new phase of rapid retreat similar to the retreat in the 1990s (Figure 2).

The rate of change in a glacier's terminus position is given by the difference between the terminus velocity and the frontal ablation rate (sum of calving and submarine melting; Truffer & Motyka, 2016). During winter, fjord water temperature decreases, subglacial discharge is minimal, and calving is subdued (Amundson et al., 2020), allowing the glacier to advance toward the morainal bank. At LeConte, the seasonal advance usually begins in late fall and typically continues until April/May but sometimes until June (Figure 3) depending on seasonal fjord and meteorological conditions (Amundson et al., 2020; Kienholz et al., 2019). Retreat is likely triggered by the onset of subglacial discharge coupled with warming of deeper, incoming fjord waters, leading to increased submarine melting (Amundson et al., 2020; Jackson et al., 2020; Motyka et al., 2003, 2013). Several processes drive the summer retreat with $U - F < 0$ (terminus velocity minus frontal ablation rate), including (1) retreat onto a reverse slope and into an overdeepened basin, increasing buoyancy and thus calving (e.g., Benn et al., 2007; van der Veen, 1996); (2) thinning caused by extensional strain and summer surface ablation further increasing buoyancy; (3) increased subglacial discharge and seasonal warming of fjord waters as well as an expansion in submarine area exposed to melting, which combine to

increase submarine melting (Motyka et al., 2003; Sutherland et al., 2019); and (4) enhanced calving from undercutting by submarine melting (O'Leary & Christoffersen, 2013).

By 2015, spring advances no longer reached the apex of MB2, signaling a potential change in terminus conditions. In 2016, the glacier experienced its largest seasonal retreat (~500 m), with the terminus reaching its farthest retracted position, to date. Spring of 2016 was relatively mild with glacier runoff beginning by early April (Amundson et al., 2020; Kienholz et al., 2019). Fjord water temperatures were also relatively warm (~5° C), increasing to 7.5°C by late August 2016 (Amundson et al., 2017, 2020; Jackson et al., 2020), suggesting that increases in submarine melting drove the large seasonal retreat. In contrast, spring of 2017 was relatively cool with a proglacial ice mélange during March and April and fjord water temperatures of ~4°C. Despite the cooler meteorological conditions and ice mélange, the terminus was unable to rebound to its previous spring position. The seasonal oscillation diminished further in 2018. However, judging from 2019–2020 Landsat images, the terminus seems to have made a renewed advance onto MB2 (Figure 3). The glacier may be continuing to grow MB2 as evidenced by the deposition of proglacial sediments in 2018 that have likely since been bulldozed onto the moraine (Figures 5, 7, and 9a).

The future stability of LeConte Glacier depends on the interplay of climate change, ocean conditions, glacier thinning, and sedimentation at the terminus. The terminus is once again in a sensitive location: at a constriction and with a right-angle bend just up-channel, both of which may promote another multiyear stillstand or perhaps even readvance. If sedimentation rates remain approximately the same, buildup of another morainal bank should be more rapid than for MB2, given that the terminus is now at a narrower location and sediment deposition is more concentrated. If built high enough (perhaps melding with MB2), the morainal bank could limit frontal ablation sufficiently to stabilize LeConte at its current position and allow a slow readvance, similar to what occurred at Taku (Brinkerhoff et al., 2017; Nolan et al., 1995) and Hubbard glaciers (Goff et al., 2012).

5.5. Relationship to Tidewater Glacier Models

Two intriguing results that have relevance for numerical modeling have come out of our work: (1) the temporary stability provided by a constriction that allows a morainal bank to develop, leading to longer-term stability; and (2) that moraine growth modifies ocean heat transport toward tidewater glacier termini by reducing terminus exposure (Figure 10), thereby affecting frontal ablation. Of the numerical models addressing tidewater glacier change, the one most closely akin to how sedimentation affects tidewater glaciers is that of Brinkerhoff et al. (2017). Their numerical model was successful in replicating the advance and retreat cycle of tidewater glaciers over decadal to centennial time scales simply by examining glacier sedimentation and development of shoal moraines. Their findings emulated the cycle even under a constant climate scenario. However, their flowline model uses simplifying assumptions; for example, it does not consider channel geometry such as constrictions and uses a simple "calving law" that does not incorporate the effects of submarine melting. Furthermore, the glacier is allowed to retreat monotonically without stillstands until reaching shallow bed at the head of its channel.

Given the detailed data on sediment flux now available for LeConte Glacier, as well as for other localities (e.g., Kehrl et al., 2011; Svalbard, Ottesen & Dowdeswell, 2006), we suggest the following avenues to expand the Brinkerhoff model: (1) incorporate channel constrictions and the dynamic sedimentary evolution of morainal banks at such pinning points, (2) include changes in ocean conditions and frontal ablation related to growth of morainal bank complexes, and (3) assess how feedbacks from these processes affect the long-term behavior of a tidewater glacier, that is, what combination of conditions would facilitate readvance versus another step retreat into a recently overdeepened basin.

6. Conclusions

LeConte Glacier formed a 100-m scale morainal bank complex (MB) between 1999 and 2017, following a 2-km rapid retreat between 1994 and 1999. Bathymetric survey data collected in 1999/2000, August 2016, May 2017, and September 2018 offer an excellent view of the dynamic evolution of these types of complex sedimentary deposits, which have historic analogs preserved subaqueously and terrestrially. Termini positions derived from satellite data show a gradual convex bowing of the ice front after the first 6 years of the stillstand, suggesting progressive vertical growth of the MB. Small 3- to 8-m-high push ridges on the back

of the MB offer evidence of seasonal readvances and bulldozing of sediment by the ice, a process that was observed to actively occur over time scales of hours to days in September 2018. The front of the MB shows signs of slumping and failure, and bedforms characteristic of cyclic steps or antidunes suggest sediment gravity flow activity within the past 2 years.

Accumulation rates in Basin A are up to ~4 m a^{-1}, representing exceptional rates of coastal sedimentation in a global context but rates typical in Alaskan fjords fed by tidewater glaciers (Cowan & Powell, 1991; Cowan et al., 2010; Goff et al., 2012; Jaeger & Nittrouer, 1999; Love et al., 2016). The annual sediment flux is estimated at 6.4×10^5 to 7.3×10^5 m^3 a^{-1}, which is at least an order of magnitude smaller than those adjacent to other temperate tidewater glaciers in the region. LeConte Glacier has previously been described as having a relatively low erosion rate due to the local bedrock lithology. Despite the relatively low sediment fluxes in the context of southeastern Alaska glaciers, these rates still represent a tremendous addition of sediment to the end moraine, whose growth reduced the area of the terminus exposed to saltwater by up to 22% in 17 years.

Despite the formation of a large morainal bank complex and stability it may offer the glacier over the time scale of years, LeConte Glacier is presently thinning, and summertime terminus positions have become increasingly retracted in the past 5 years. Though moraines are often cited as a necessary condition for renewed advance in the tidewater glacier cycle, LeConte may serve as a case study of numerous tidewater glacier systems where a growing MB has been insufficient to permit renewed advance, due to a variety of other forcing factors. Our observations suggest that temporary glacier stability provided by pinning points in fjords can allow large moraines to form, even during long-term glacier retreat and that these moraines provide additional terminus stability and can postpone retreat, even if they cannot facilitate renewed advance. Once initiated, retreat from a newly formed moraine is likely to be quick due to unstable retreat into an overdeepened basin that is created in concert with the formation of a morainal bank complex. In other words, fjord geometry, ocean conditions, and sediment dynamics act together to create pulses in terminus retreat. The ability of a moraine to modify glacier retreat patterns will depend on erosion and sedimentation rates, which can be variable.

Data Availability Statement

ADCP, CTD, and grain-size data are available at https://data.nodc.noaa.gov/ under NOAA NCEI Accession 0189574 (https://accession.nodc.noaa.gov/0189574). Multibeam and CHIRP data are archived under DOIs https://doi.org/10.5281/zenodo.3383318 and https://doi.org/10.5281/zenodo.4008565, respectively.

Acknowledgments

This work was supported by NSF Arctic Natural Sciences Grants OPP—1503910, 1504191, 1504288, and 1504521. National Geographic CP4-171R-17 to E. Pettit and J. Nash helped support 2018 cruise logistics. We thank Jonathan Nash, Rebecca Jackson, Pat Dryer, June Marion, John Mickett, Dylan Winters, Jasmine Nahorniak, Erin Pettit, Anna Simpson, Akua McLeod, and the crew of the M/V Steller, M/V Amber Anne, and R/V Pelican for their field assistance. We thank Petersburg High School and the U.S. Forest Service for accommodating this project. We also wish to thank the Shtax'héen Kwáan Tlingits, whose ancestral lands lie in this region. We also thank Charles Nittrouer (UW), Michele Koppes (UBC), and Tony Rodriguez (UNC IMS) for providing sediment sampling equipment, CHIRP equipment, and sonar processing assistance, as well as OSU CEOAS for providing grain-size analysis facilities. We also thank John Jaeger, two anonymous reviewers, and the Associate Editor who provided feedback on the manuscript.

References

Åkesson, H., Nisancioglu, K. H., & Nick, F. M. (2018). Impact of fjord geometry on grounding line stability. *Frontiers in Earth Science*, *6*, 119–116. http://doi.org/10.3389/feart.2018.00071

Alley, R. B. (1991). Sedimentary processes may cause fluctuations of tidewater glaciers. *Annals of Glaciology*, *15*, 119–124. http://doi.org/10.3189/1991aog15-1-115-121

Alley, R. B., Blankenship, D. D., Bentley, C. R., & Rooney, S. T. (1987). Till beneath ice stream B: 3. Till deformation: Evidence and implications. *Journal of Geophysical Research*, *92*(B9), 8921–8929.

Amundson, J. (2016). A mass-flux perspective of the tidewater glacier cycle. *Journal of Glaciology*, *62*(231), 82–93. https://doi.org/10.1017/jog.2016.14

Amundson, J., Kienholz, C., Motyka, R., Sutherland, D., Nash, J., Jackson, R., & Carroll, D. (2017). Collaborative research: Impact of subglacial discharge on turbulent plume dynamics and ocean-glacier heat and mass transfer, Southeast Alaska, 2016–2017, Arctic Data Center. https://doi.org/10.18739/A22G44

Amundson, J. M., & Carroll, D. (2018). Effect of topography on subglacial discharge and submarine melting during tidewater glacier retreat. *Journal of Geophysical Research: Earth Surface*, *123*, 66–79. http://doi.org/10.1002/2017JF004376

Amundson, J. M., Kienholz, C., Hager, A. O., Jackson, R. H., Motyka, R. J., Nash, J. D., & Sutherland, D. A. (2020). Formation, flow, and break-up of ephemeral ice mélange at LeConte Glacier and Bay, Alaska. *Journal of Glaciology*. In production, *66*(258), 577–590. https://doi.org/10.1017/jog.2020.29

Anderson, J. B. (1999). *Antarctic marine geology*. Cambridge: Cambridge University Press. https://doi.org/10.1017/CBO9780511759376

Arendt, A., Echelmeyer, K., Harrison, W., Lingle, C., & Valentine, V. (2002). Rapid wastage of Alaska glaciers and their contribution to rising sea level. *Science*, *297*(5580), 382–386. https://doi.org/10.1126/science.1072497

Barclay, D. J., Calkin, P. E., & Wiles, G. C. (2001). Holocene history of Hubbard Glacier in Yakutat Bay and Russell Fiord, southern Alaska. *Geological Society of America Bulletin*, *113*(3), 388–402. https://doi.org/10.1130/0016-7606(2001)113<0388:HHOHGI>2.0.CO;2

Benn, D. I., Warren, C. R., & Mottram, R. H. (2007). Calving processes and the dynamics of calving glaciers. *Earth-Science Reviews*, *82*(3–4), 143–179. https://doi.org/10.1016/j.earscirev.2007.02.002

Bennett, M. R. (2001). The morphology, structural evolution and significance of push moraines. *Earth-Science Reviews*, *53*(3–4), 197–236. https://doi.org/10.1016/S0012-8252(00)00039-8

Berthier, E., Larsen, C., Durkin, W. J., Willis, M. J., & Pritchard, M. E. (2018). Brief communication: Unabated wastage of the Juneau and Stikine icefields (southeast Alaska) in the early 21st century. *The Cryosphere*, *12*(4), 1523–1530. https://doi.org/10.5194/tc-12-1523-2018

Boldt, K. V., Nittrouer, C. A., Hallet, B., Koppes, M. N., Forrest, B. K., Wellner, J. S., & Anderson, J. B. (2013). Modern rates of glacial sediment accumulation along a 15° S-N transect in fjords from the Antarctic Peninsula to southern Chile. *Journal of Geophysical Research: Earth Surface*, *118*, 2072–2088. https://doi.org/10.1002/jgrf.20145

Boulton, G. S. (1986). Push-moraines and glacier-contact fans in marine and terrestrial environments. *Sedimentology*, *33*, 667–698.

Boulton, G. S. (1990). Sedimentary and sea level changes during glacial cycles and their control on glacimarine facies architecture. *Geological Society, London, Special Publications*, *53*(1), 15–52. https://doi.org/10.1144/GSL.SP.1990.053.01.02

Boulton, G. S., Van der Meer, J. J. M., Hart, J., Beets, D., Ruegg, G. H. J., Van der Wateren, F. M., & Jarvis, J. (1996). Till and moraine emplacement in a deforming bed surge—An example from a marine environment. *Quaternary Science Reviews*, *15*(10), 961–987. https://doi.org/10.1016/0277-3791(95)00091-7

Brew, D. A., & Friedman, R. M. (2002). Notes on the bedrock geology and geography of the Stikine Icefield, Coast Mountains Complex, southeastern Alaska. Chapt. 5, U.S. Geological Survey. *Professional Paper*, *1662*, 77–86.

Brinkerhoff, D., Truffer, M., & Aschwanden, A. (2017). Sediment transport drives tidewater glacier periodicity. *Nature Communications*, *8*(1), 90–98. http://doi.org/10.1038/s41467-017-00095-5

Burton, D. J., Dowdeswell, J. A., Hogan, K. A., & Noormets, R. (2016). Marginal fluctuations of a Svalbard surge-type tidewater glacier, Blomstrandbreen, since the Little Ice Age: A record of three surges. *Arctic, Antarctic, and Alpine Research*, *48*(2), 411–426. https://doi.org/10.1657/AAAR0014-094

Cai, J., Powell, R. D., Cowan, E. A., & Carlson, P. R. (1997). Lithofacies and seismic-reflection interpretation of temperate glacimarine sedimentation in Tarr Inlet, Glacier Bay, Alaska. *Marine Geology*, *143*(1–4), 5–37. https://doi.org/10.1016/S0025-3227(97)00088-1

Caress, D. W., Chayes, D. N., & dos Santos Ferreira, C. (2018). MB-system seafloor mapping software: Processing and display of swath sonar data. Monterey Bay Aquarium Research Institute, https://www.mbari.org/products/research-software/mb-system/, [accessed 18 Apr 2019].

Carr, J. R., Stokes, C., & Vieli, A. (2014). Recent retreat of major outlet glaciers on Novaya Zemlya, Russian Arctic, influenced by fjord geometry and sea-ice conditions. *Journal of Glaciology*, *60*(219), 155–170. https://doi.org/10.3189/2014JoG13J122

Catania, G. A., Stearns, L. A., Sutherland, D. A., Fried, M. J., Bartholomaus, T. C., Morlighem, M., et al. (2018). Geometric controls on tidewater glacier retreat in central western Greenland. *Journal of Geophysical Research: Earth Surface*, *123*, 2024–2038. https://doi.org/10.1029/2017JF004499

Clare, M. A., Clarke, J. H., Talling, P. J., Cartigny, M. J., & Pratomo, D. G. (2016). Preconditioning and triggering of offshore slope failures and turbidity currents revealed by most detailed monitoring yet at a fjord-head delta. *Earth and Planetary Science Letters*, *450*, 208–220. https://doi.org/10.1016/j.epsl.2016.06.021

Cowan, E. A., Carlson, P. R., & Powell, R. D. (1996). The marine record of the Russell Fiord outburst flood, Alaska, USA. *Annals of Glaciology*, *22*, 194–199.

Cowan, E. A., & Powell, R. D. (1991). Ice-proximal sediment accumulation rates in a temperate glacial fjord, southeastern Alaska. *Glacial marine sedimentation*, 61–73.

Cowan, E. A., Powell, R. D., & Smith, N. D. (1988). Rainstorm-induced event sedimentation at the tidewater front of a temperate glacier. *Geology*, *16*(5), 409–412. https://doi.org/10.1130/0091-7613(1988)016<0409:RIESAT>2.3.CO;2

Cowan, E. A., Seramur, K. C., Cai, J., & Powell, R. D. (1999). Cyclic sedimentation produced by fluctuations in meltwater discharge, tides and marine productivity in an Alaskan fjord. *Sedimentology*, *46*(6), 1109–1126.

Cowan, E. A., Seramur, K. C., Powell, R. D., Willems, B. A., Gulick, S. P., & Jaeger, J. M. (2010). Fjords as temporary sediment traps: History of glacial erosion and deposition in Muir Inlet, Glacier Bay National Park, southeastern Alaska. *GSA Bulletin*, *122*(7–8), 1067–1080. https://doi.org/10.1130/B26595.1

Csatho, B., Schenk, T., Van der Veen, C. J., & Krabill, W. B. (2008). Intermittent thinning of Jakobshavn Isbræ, West Greenland, since the Little Ice Age. *Journal of Glaciology*, *54*(184), 131–144. https://doi.org/10.3189/002214308784409035

Curran, K. J., Hill, P. S., Milligan, T. G., Cowan, E. A., Syvitski, J. P. M., & Konings, S. M. (2004). Fine-grained sediment flocculation below the Hubbard Glacier meltwater plume, Disenchantment Bay, Alaska. *Marine Geology*, *203*(1–2), 83–94. https://doi.org/10.1016/S0025-3227(03)00327-X

Dowdeswell, J. A., Hogan, K. A., Arnold, N. S., Mugford, R. I., Wells, M., Hirst, J. P. P., & Decalf, C. (2015). Sediment-rich meltwater plumes and ice-proximal fans at the margins of modern and ancient tidewater glaciers: Observations and modelling. *Sedimentology*, *62*(6), 1665–1692. http://doi.org/10.1111/sed.12198

Dowdeswell, J. A., & Vásquez, M. (2013). Submarine landforms in the fjords of southern Chile: Implications for glacimarine processes and sedimentation in a mild glacier-influenced environment. *Quaternary Science Reviews*, *64*(C), 1–19. http://doi.org/10.1016/j.quascirev.2012.12.003

Eidam, E. F., Nittrouer, C. A., Lundesgaard, Ø., Homolka, K. K., & Smith, C. R. (2019). Variability of sediment accumulation rates in an Antarctic fjord. *Geophysical Research Letters*, *46*, 13,271–13,280. https://doi.org/10.1029/2019GL084499

Elverhøi, A., Liestol, O., & Nagy, J. (1980). Glacial erosion, sedimentation and microfauna in the inner part of Kongs-fjorden, Spitsbergen. Geological and geophysical research in Svalbard and on Jan Mayen, 1980. *Norsk Polarinstitutt Skrifter*, *172*, 33–60. Oslo: Norwegian Polar Institute.

Elverhøi, A., Lønne, Ø., & Seland, R. (1983). Glaciomarine sedimentation in a modern fjord environment, Spitsbergen. *Polar Research*, *1*(2), 127–150. https://doi.org/10.1111/j.1751-8369.1983.tb00697.x

Fischer, M. P., & Powell, R. D. (1998). A simple model for the influence of push-morainal banks on the calving and stability of glacial tidewater termini. *Journal of Glaciology*, *44*(146), 31–41. http://doi.org/10.3189/s002214300000232x

Fricke, A. T., Sheets, B. A., Nittrouer, C. A., Allison, M. A., & Ogston, A. S. (2015). An examination of Froude-supercritical flows and cyclic steps on a subaqueous lacustrine delta, Lake Chelan, Washington, USA. *Journal of Sedimentary Research*, *85*(7), 754–767. https://doi.org/10.2110/jsr.2015.48

Goff, J. A., Lawson, D. E., Willems, B. A., Davis, M., & Gulick, S. P. S. (2012). Morainal bank progradation and sediment accumulation in Disenchantment Bay, Alaska: Response to advancing Hubbard Glacier. *Journal of Geophysical Research*, *117*, F02031. http://doi.org/10.1029/2011JF002312

Hallet, B., Hunter, L., & Bogen, J. (1996). Rates of erosion and sediment evacuation by glaciers: A review of field data and their implications. *Global and Planetary Change*, *12*(1–4), 213–235. http://doi.org/10.1016/0921-8181(95)00021-6

Hoek, E., & Bray, J. W. (1981). *Rock slope engineering* (3rd ed., Vol. 358). London: Institution of Mining and Metallurgy.

Holmlund, P., & Fuenzalida, H. (1995). Anomalous glacier responses to 20th century climatic changes in Darwin Cordillera, southern Chile. *Journal of Glaciology*, *41*(139), 465–473. https://doi.org/10.1017/S0022143000034808

Howat, I. M., & Eddy, A. (2011). Multi-decadal retreat of Greenland's marine-terminating glaciers. *Journal of Glaciology*, *57*(203), 389–396. https://doi.org/10.3189/002214311796905631

Hughes Clarke, J. E. (2016). First wide-angle view of channelized turbidity currents links migrating cyclic steps to flow characteristics. *Nature Communications*, *7*(1), 1–13. http://doi.org/10.1038/ncomms11896

Hunter, L. E., Powell, R. D., & Lawson, D. E. (1996a). Flux of debris transported by ice at three Alaskan tidewater glaciers. *Journal of Glaciology*, *42*(140), 123–135. http://doi.org/10.3189/S0022143000030586

Hunter, L. E., Powell, R. D., & Lawson, D. E. (1996b). Morainal-bank sediment budgets and their influence on the stability of tidewater termini of valley glaciers entering Glacier Bay, Alaska, U.S.A. *Annals of Glaciology*, *22*, 211–216. http://doi.org/10.3189/1996AoG22-1-211-216

Jackson, R. H., Nash, J. D., Kienholz, C., Sutherland, D. A., Amundson, J. A., Motyka, R. J., et al. (2020). Concentrated meltwater intrusions reveal mechanisms for rapid glacier melt. *Geophysical Research Letters*, *47*, e2019GL085335. https://doi.org/10.1029/2019GL085335

Jaeger, J. M., & Nittrouer, C. A. (1999). Sediment deposition in an Alaskan fjord; controls on the formation and preservation of sedimentary structures in Icy Bay. *Journal of Sedimentary Research*, *69*(5), 1011–1026. https://doi.org/10.2110/jsr.69.1011

Johnson, M. D., Benediktsson, Í. Ö., & Björklund, L. (2013). The Ledsjö end moraine—A subaquatic push moraine composed of glacio-marine clay in central Sweden. *Proceedings of the Geologists Association*, *124*, 738–752.

Kehrl, L. M., Hawley, R. L., Powell, R. D., & Brigham-Grette, J. (2011). Glacimarine sedimentation processes at Kronebreen and Kongsvegen, Svalbard. *Journal of Glaciology*, *57*(205), 841–847. http://doi.org/10.3189/002214311798043708

Kienholz, C., Amundson, J. M., Motyka, R. J., Jackson, R. H., Mickett, J. B., Sutherland, D. A., et al. (2019). Tracking icebergs with time-lapse photography and sparse optical flow, LeConte Bay, Alaska, 2016–2017. *Journal of Glaciology*, *65*(250), 195–211. https://doi.org/10.1017/jog.2018.105

Kienholz, C., Herreid, S., Rich, J. L., Arendt, A. A., Hock, R., & Burgess, E. W. (2015). Derivation and analysis of a complete modern-date glacier inventory for Alaska and northwest Canada. *Journal of Glaciology*, *61*(227), 403–420.

Koppes, M., Hallet, B., & Anderson, J. (2009). Synchronous acceleration of ice loss and glacial erosion, Glaciar Marinelli, Chilean Tierra del Fuego. *Journal of Glaciology*, *55*(190), 207–220. https://doi.org/10.3189/002214309788608796

Koppes, M., Sylwester, R., Rivera, A., & Hallet, B. (2010). Variations in sediment yield over the advance and retreat of a calving glacier, Laguna San Rafael, North Patagonian Icefield. *Quaternary Research*, *73*(1), 84–95. https://doi.org/10.1016/j.yqres.2009.07.006

Kristensen, L., Benn, D. I., Hormes, A., & Ottesen, D. (2009). Mud aprons in front of Svalbard surge moraines: Evidence of subglacial deforming layers or proglacial glaciotectonics? *Geomorphology*, *111*(3–4), 206–221. https://doi.org/10.1016/j.geomorph.2009.04.022

Kuriger, E. M., Truffer, M., Motyka, R. J., & Bucki, A. K. (2006). Episodic reactivation of large-scale push moraines in front of the advancing Taku Glacier, Alaska. *Journal of Geophysical Research*, *111*, F01009. https://doi.org/10.1029/2005JF000385

Larsen, C. F., Burgess, E., Arendt, A. A., O'neel, S., Johnson, A. J., & Kienholz, C. (2015). Surface melt dominates Alaska glacier mass balance. *Geophysical Research Letters*, *42*, 5902–5908. https://doi.org/10.1002/2015GL064349

Larsen, C. F., Motyka, R. J., Arendt, A. A., Echelmeyer, K. A., & Geissler, P. E. (2007). Glacier changes in southeast Alaska and northwest British Columbia and contribution to sea level rise. *Journal of Geophysical Research*, *112*, F01007. https://doi.org/10.1029/2006JF000586

Larter, R. D., & Barker, P. F. (1989). Seismic stratigraphy of the Antarctic Peninsula Pacific margin: A record of Pliocene-Pleistocene ice volume and paleoclimate. *Geology*, *17*(8), 731. http://doi.org/10.1130/0091-76131989)017<0731:ssotap>2.3.co;2

Lastras, G., & Dowdeswell, J. A. (2016). Terminal and recessional moraines in the fjords of southern Chile. *Geological Society, London, Memoirs*, *46*(1), 65–66. https://doi.org/10.1144/M46.29

Love, K. B., Hallet, B., Pratt, T. L., & O'Neel, S. (2016). Observations and modeling of fjord sedimentation during the 30 year retreat of Columbia Glacier, AK. *Journal of Glaciology*, *62*(234), 778–793. http://doi.org/10.1017/jog.2016.67

McNabb, R. W., & Hock, R. (2014). Alaska tidewater glacier terminus positions, 1948–2012. *Journal of Geophysical Research: Earth Surface*, *119*, 153–167. http://doi.org/10.1002/2013JF002915

McNabb, R. W., Hock, R., & Huss, M. (2015). Variations in Alaska tidewater glacier frontal ablation, 1985-2013. *Journal of Geophysical Research: Earth Surface*, *120*, 120–136. http://doi.org/10.1002/2014JF003276

Meier, M. E., & Post, A. (1987). Fast tidewater glaciers. *Journal of Geophysical Research*, *92*(B9), 9051–9058. https://doi.org/10.1029/JB092iB09p09051

Melkonian, A. K., Willis, M. J., & Pritchard, M. E. (2016). Stikine icefield mass loss between 2000 and 2013/2014. *Frontiers in Earth Science*, *4*(63), 2838–2812. http://doi.org/10.3389/feart.2016.000893

Mercer, J. H. (1961). The response of fjord glaciers to changes in the firn limit. *Journal of Glaciology*, *3*(29), 850–858.

Meslard, F., Bourrin, F., Many, G., & Kerhervé, P. (2018). Suspended particle dynamics and fluxes in an Arctic fjord (Kongsfjorden, Svalbard). *Estuarine*, *204*, 212–224. http://doi.org/10.1016/j.ecss.2018.02.020

Motyka, R. J., Begét, J. E., & Bowen, P. (1998). Recent retreat of LeConte Glacier and associated calving and iceberg hazards. *Alaska Division of Geological & Geophysical Surveys Representative Investment*, 98–15.

Motyka, R. J., Cassotto, R., Truffer, M., Kjeldsen, K. K., Van As, D., Korsgaard, N. J., et al. (2017). Asynchronous behavior of outlet glaciers feeding Godthåbsfjord (Nuup Kangerlua) and the triggering of Narsap Sermia's retreat in SW Greenland. *Journal of Glaciology*, *63*(238), 288–308. https://doi.org/10.1017/jog.2016.138

Motyka, R. J., Dryer, W. P., Amundson, J., Truffer, M., & Fahnestock, M. (2013). Rapid submarine melting driven by subglacial discharge, LeConte Glacier, Alaska. *Geophysical Research Letters*, *40*, 5153–5158. http://doi.org/10.1002/grl.51011

Motyka, R. J., Hunter, L., Echelmeyer, K. A., & Connor, C. (2003). Submarine melting at the terminus of a temperate tidewater glacier, LeConte Glacier, Alaska, U.S.A. *Annals of Glaciology*, *36*, 57–65. http://doi.org/10.3189/172756403781816374

Motyka, R. J., Truffer, M., Kuriger, E. M., & Bucki, A. K. (2006). Rapid erosion of soft sediments by tidewater glacier advances: Taku Glacier, Alaska, USA. *Geophysical Research Letters*, *33*, L24504. https://doi.org/10.1029/2006GL028467

Nick, F. M., van der Veen, C. J., & Oerlemans, J. (2007). Controls on advance of tidewater glaciers: Results from numerical modeling applied to Columbia Glacier. *Journal of Geophysical Research*, *112*, F03S24. https://doi.org/10.1029/2006JF000551

Nolan, M., Motyka, R. J., Echelmeyer, K. A., & Trabant, D. (1995). Ice-thickness measurements of Taku Glacier, Alaska, U.S.A., and their relevance to its recent behaviour. *Journal of Glaciology*, *41*(139), 541–553.

Normandeau, A., Lajeunesse, P., Poiré, A. G., & Francus, P. (2016). Morphological expression of bedforms formed by supercritical sediment density flows on four fjord-lake deltas of the south-eastern Canadian Shield (Eastern Canada). *Sedimentology*, *63*(7), 2106–2129. https://doi.org/10.1111/sed.12298

Oerlemans, J., & Nick, F. M. (2006). Modelling the advance–retreat cycle of a tidewater glacier with simple sediment dynamics. *Global and Planetary Change*, *50*(3–4), 148–160. http://doi.org/10.1016/j.gloplacha.2005.12.002

O'Leary, M., & Christoffersen, P. (2013). Calving on tidewater glaciers amplified by submarine frontal melting. *The Cryosphere*, *7*(1), 119–128. https://doi.org/10.5194/tc-7-119-2013

O'Neel, S., Echelmeyer, K. A., & Motyka, R. J. (2001). Short-term flow dynamics of a retreating tidewater glacier: LeConte Glacier, Alaska, U.S.A. *Journal of Glaciology*, *47*(159), 567–578. https://doi.org/10.3189/172756501781831855

O'Neel, S., Echelmeyer, K. A., & Motyka, R. J. (2003). Short-term variations in calving of a tidewater glacier: LeConte Glacier, Alaska, U.S. A. *Journal of Glaciology*, *49*(167), 587–598. http://doi.org/10.3189/172756503781830430
Ottesen, D., & Dowdeswell, J. A. (2006). Assemblages of submarine landforms produced by tidewater glaciers in Svalbard. *Journal of Geophysical Research*, *111*, F01016. http://doi.org/10.1029/2005JF000330
Overeem, I., Hudson, B. D., Syvitski, J. P., Mikkelsen, A. B., Hasholt, B., van den Broeke, M. R., et al. (2017). Substantial export of suspended sediment to the global oceans from glacial erosion in Greenland. *Nature Geoscience*, *10*(11), 859–863. https://doi.org/10.1038/ngeo3046
Pelto, M. S., Mcgee, S. R., Adema, G. W., Beedle, M. J., Miller, M. M., Sprenke, K. F., & Lang, M. (2008). The equilibrium flow and mass balance of the Taku Glacier, Alaska 1950–2006. The cryosphere discussions. *Copernicus*, *2*(3), 275–298.
Pfirman, S. L., & Solheim, A. (1989). Subglacial meltwater discharge in the open-marine tidewater glacier environment: Observations from Nordaustlandet, Svalbard Archipelago. *Marine Geology*, *86*(4), 265–281. http://doi.org/10.1016/0025-3227(89)90089-3
Post, A. (1975). *Preliminary hydrology and historic terminal changes of Columbia Glacier, Alaska*. Washington, DC: U.S. Geological Survey Hydrological Investigation Atlas, HA-559, 3 sheets, scale 1:10,000.
Post, A., & Motyka, R. J. (1995). Taku and LeConte glaciers, Alaska: Calving-speed control of late-Holocene asynchronous advances and retreats. *Physical Geography*, *16*(1), 59–82. http://doi.org/10.1080/02723646.1995.10642543
Post, A., O'Neel, S., Motyka, R. J., & Streveler, G. (2011). A complex relationship between calving glaciers and climate. *Eos Transactions American Geophysical Union*, *92*(37), 305. https://doi.org/10.1029/2011EO370001
Powell, R. D. (1984). Glacimarine processes and inductive lithofacies modelling of ice shelf and tidewater glacier sediments based on Quaternary examples. *Marine Geology*, *57*(1–4), 1–52. https://doi.org/10.1016/0025-3227(84)90194-4
Powell, R. D. (1990). Glacimarine processes at grounding-line fans and their growth to ice-contact deltas. *Geological Society, London, Special Publications*, *53*(1), 53–73. http://doi.org/10.1144/gsl.sp.1990.053.01.03
Powell, R. D. (1991). Grounding-line systems as second-order controls on fluctuations of tidewater termini of temperate glaciers. In J. B. Anderson & G. M. Ashley (Eds.), *Glacial marine sedimentation; Paleoclimatic significance* (Vol. 261, pp. 75–93). Boulder, Colorado: Geological Society of America Special Paper 261. https://doi.org/10.1130/SPE261-p75
Powell, R. D., & Molnia, B. F. (1989). Glacimarine sedimentary processes, facies and morphology of the south-southeast Alaska shelf and fjords. *Marine Geology*, *85*(2–4), 359–390.
Ritchie, B., Lingle, C. S., Motyka, R. J., & Truffer, M. (2008). Seasonal fluctuations in the advance of a tidewater glacier and potential causes: Hubbard Glacier, Alaska, USA. *Journal of Glaciology*, *54*(186), 401–411. https://doi.org/10.3189/002214308785836977
Schimel, A. C., Ierodiaconou, D., Hulands, L., & Kennedy, D. M. (2015). Accounting for uncertainty in volumes of seabed change measured with repeat multibeam sonar surveys. *Continental Shelf Research*, *111*, 52–68. https://doi.org/10.1016/j.csr.2015.10.019
Seramur, K. C., Powell, R. D., & Carlson, P. R. (1997). Evaluation of conditions along the grounding line of temperate marine glaciers: An example from Muir Inlet, Glacier Bay, Alaska. *Marine Geology*, *140*(3–4), 307–327. http://doi.org/10.1016/s0025-3227(97)00026-1
Smith, D. P., Ruiz, G., Kvitek, R., & Iampietro, P. J. (2005). Semiannual patterns of erosion and deposition in upper Monterey Canyon from serial multibeam bathymetry. *Geological Society of America Bulletin*, *117*(9), 1123–1133. https://doi.org/10.1130/B25510.1
Smith, J. N., & Walton, A. (1980). Sediment accumulation rates and geochronologies measured in the Saguenay Fjord using the Pb-210 dating method. *Geochimica et Cosmochimica Acta*, *44*(2), 225–240. https://doi.org/10.1016/0016-7037(80)90134-9
Sohn, H. G., Jezek, K. C., & van der Veen, C. J. (1998). Jakobshavn Glacier, West Greenland: 30 years of spaceborne observations. *Geophysical Research Letters*, *25*(14), 2699–2702. https://doi.org/10.1029/98GL01973
Stearns, L. A., Hamilton, G. S., van der Veen, C. J., Finnegan, D. C., O'Neel, S., Scheick, J. B., & Lawson, D. E. (2015). Glaciological and marine geological controls on terminus dynamics of Hubbard Glacier, southeast Alaska. *Journal of Geophysical Research: Earth Surface*, *120*, 1065–1081. https://doi.org/10.1002/2014JF003341
Streuff, K., Cofaigh, C., Noormets, R., & Lloyd, J. M. (2018). Submarine landform assemblages and sedimentary processes in front of Spitsbergen tidewater glaciers. *Marine Geology*, *402*, 209–227. https://doi.org/10.1016/j.margeo.2017.09.006
Sutherland, D. A., Jackson, R. H., Kienholz, C., Amundson, J. M., Dryer, W. P., Duncan, C., et al. (2019). Direct observations of submarine melt and subsurface geometry at a tidewater glacier. *Science*, *365*(6451), 369–374. https://doi.org/10.1126/science.aax3528
Syvitski, J. P., Burrell, D. C., & Skei, J. M. (1987). *Fjords: Processes and products*. New York: Springer-Verlag. https://doi.org/10.1007/978-1-4612-4632-9
Syvitski, J. P. M. (1989). On the deposition of sediment within glacier-influenced fjords: Oceanographic controls. *Marine Geology*, *85*(2–4), 301–329. http://doi.org/10.1016/0025-3227(89)90158-8
Trabant, D. C., Krimmel, R. M., Echelmeyer, K. A., Zirnheld, S. L., & Elsberg, D. H. (2003). The slow advance of a calving glacier: Hubbard Glacier, Alaska, USA. *Annals of Glaciology*, *36*, 45–50. https://doi.org/10.3189/172756403781816400
Truffer, M., & Motyka, R. J. (2016). Where glaciers meet water: Subaqueous melt and its relevance to glaciers in various settings. *Reviews of Geophysics*, *54*, 220–239. https://doi.org/10.1002/2015RG000494
Truffer, M. A., Motyka, R. J., Harrison, W. D., Echelmeyer, K. A., Fisk, B., & Tulaczyk, S. L. (1999). Subglacier drilling at Black Rapids Glacier, Alaska, USA: Drilling method and sample descriptions. *Journal of Glaciology*, *45*(151), 495–505. https://doi.org/10.1017/S0022143000001350
Trusel, L. (2009). Inferences into glacimarine sedimentary dynamics, processes, and environments from multibeam sonar records in Alaskan fjords, MS thesis, Dept. of Geol. and Environ. Geosci., Northern Illinois Univ., DeKalb, Ill.
van der Veen, C. J. (1996). Tidewater calving. *Journal of Glaciology*, *42*(141), 375–385. https://doi.org/10.1017/S0022143000004226
Viens, R. J. (2001). Late Holocene climate change and calving glacier fluctuations along the southwestern margin of the Stikine Icefield, Alaska. Ph.D. dissertation, U. of Washington, 160 p.
Willems, B. A., Powell, R. D., Cowan, E. A., & Jaeger, J. M. (2011). Glacial outburst flood sediments within Disenchantment Bay, Alaska: Implications of recognizing marine jökulhlaup deposits in the stratigraphic record. *Marine Geology*, *284*(1–4), 1–12. https://doi.org/10.1016/j.margeo.2011.03.004

Reference From the Supporting Information

Lepland, A., Bøe, R., Lepland, A., & Totland, O. (2009). Monitoring the volume and lateral spread of disposed sediments by acoustic methods, Oslo Harbor, Norway. *Journal of Environmental Management*, *90*(11), 3589–3598. https://doi.org/10.1016/j.jenvman.2009.06.013